

1 **An observational study of the effects of aerosols on diurnal variation of heavy rainfall**
2 **and associated clouds over Beijing-Tianjin-Hebei**

3
4 Siyuan Zhou^{1,2,3}, Jing Yang^{1,2*}, Wei-Chyung Wang³, Chuanfeng Zhao⁴, Daoyi Gong^{1,2}, Peijun Shi^{1,2}

5
6 ¹ State Key Laboratory of Earth Surface Process and Resource Ecology, Beijing Normal University, China

7 ² Key Laboratory of Environmental Change and Natural Disaster, Faculty of Geographical Science, Beijing
8 Normal University, China

9 ³ Atmospheric Sciences Research Center, State University of New York, Albany, New York 12203, USA

10 ⁴ College of Global Change and Earth System Science, Beijing Normal University, China

11
12
13 Submitted to ACP

14 Oct 2018
15
16
17
18
19
20
21
22
23
24
25
26
27
28
29
30
31
32

33 *Correspondence to: Jing Yang, State Key Laboratory of Earth Surface Process and Resource Ecology/ Key
34 Laboratory of Environmental Change and Natural Disaster, Faculty of Geographical Science, Beijing Normal
35 University, 19#Xinjiekouwai Street, Haidian District, Beijing 100875, China. E-mail: yangjing@bnu.edu.cn

36 **Abstract:** Our previous study found that the observed rainfall diurnal variation over Beijing-Tianjin-Hebei
37 shows distinct signature of the effects of pollutants. Here we used the hourly rainfall data together with
38 satellite-based daily information of aerosols and clouds to further investigate changes in heavy rainfall and
39 clouds associated with aerosol changes. Because of the strong coupling effects, we also examined the
40 sensitivity of these changes to moisture (specific humidity) variations. For heavy rainfall, three distinguished
41 characteristics are identified: *earlier start time*, *earlier peak time*, and *longer duration*; and the signals are
42 robust using aerosol indicators based on both aerosol optical depth and cloud droplet number concentration.
43 In-depth analysis reveals that the first two characteristics occur in the presence of (absorbing) black carbon
44 aerosols and that the third is related to more (scattering) sulfate aerosols and sensitive to moisture abundance.
45 Cloud changes are also evident, showing increases in cloud fraction, cloud top pressure, the liquid/ice cloud
46 optical thickness and cloud water path, and decrease in ice cloud effective radius; and these changes are
47 insensitive to moisture. Finally, the mechanisms for heavy rainfall characteristics are discussed and
48 hypothesized.

49 **Key words:** aerosol, heavy rainfall, diurnal variation, cloud, Beijing-Tianjin-Hebei, observational study

50

51 **1. Introduction**

52 Aerosols modify the hydrologic cycle through direct radiative and indirect cloud adjustment effects (IPCC,
53 2013). The direct effect, through absorbing and scattering solar radiation, leads to heating in the atmosphere
54 (e.g. Jacobson 2001; Lau et al. 2006) and cooling on the surface (Lelieveld and Heintzenberg 1992; Guo et al.
55 2013; Yang et al., 2018), causing changes in atmospheric vertical static stability and subsequently modulation
56 of rainfall (e.g. Rosenfeld et al. 2008). On the other hand, water-soluble aerosols serving as cloud
57 condensation nuclei (CCN) affect the warm-rain and cold-rain processes through influencing the cloud droplet
58 size distributions, cloud top heights and other cloud properties (Jiang et al., 2002; Givati and Rosenfeld 2004;
59 Chen et al., 2011; Lim and Hong 2012; Tao et al., 2012). For Beijing-Tianjin-Hebei (BTH) the significant
60 increase in pollution in recent decades has raised issues concerning aerosol-radiation-cloud-precipitation
61 interactions. While the impact of aerosols on light rainfall or warm-rain processes is in general agreement
62 among studies for this region (e.g., Qian et al., 2009), the uncertainties of the effects on heavy convective
63 rainfall are still large (Guo et al., 2014; Wang et al., 2016).

64 The clouds that can generate heavy convective rainfall in BTH region usually contain warm clouds, cold
65 clouds and mixed-phase clouds (e.g. Guo et al., 2015). Because the aerosol-cloud interactions in different
66 types of clouds are distinct (Gryspeerdt et al., 2014b), aerosol indirect effect during heavy rainfall is more
67 complicated than its direct effect (Sassen et al., 1995; Sherwood, 2002; Jiang et al., 2008, Tao et al., 2012).
68 For warm clouds, by serving as CCN that nucleates more cloud droplets, aerosols can increase cloud albedo so
69 called albedo effect or Twomey effect (Twomey, 1977), lengthen the cloud lifetime so called lifetime effect

70 (Albrecht, 1989), and enhance thin cloud thermal emissivity so called thermal emissivity effect (Garrett and
71 Zhao, 2006). The above effects tend to increase the cloud microphysical stability and suppress warm-rain
72 processes (Albrecht 1989; Rosenfeld et al. 2014). For cold clouds and mixed-phase clouds, many studies
73 reported that the cloud liquid accumulated by aerosols is converted to ice hydrometeors above the freezing
74 level, which invigorates deep convective clouds and intensifies heavy precipitation so called invigoration
75 effect (Rosenfeld and Woodley, 2000; Rosenfeld et al., 2008; Lee et al. 2009; Guo et al. 2014). The Twomey
76 effect infers that aerosols serving as CCN that increase the cloud droplets could reduce cloud droplet size
77 within a constant liquid water path (Twomey, 1977). However, the opposite results of relationship between
78 aerosols and cloud droplet effective radius were reported in observations (Yuan et al., 2008; Panicker et al.,
79 2010; Jung et al., 2013; Harikishan et al., 2016; Qiu et al., 2017), which might be related with the moisture
80 supply near the cloud base (Yuan et al., 2008; Qiu et al., 2017). Besides, the influence of aerosols on ice
81 clouds also depends upon the amount of moisture supply (Jiang et al., 2008). Therefore, how the aerosols
82 modify the heavy convective rainfall and associated cloud changes does not reach a consensus, particularly if
83 considering the different moisture conditions.

84 Heavy convective rainfall over BTH region usually occurs within a few hours, thus studying on the
85 relationship between aerosols and rainfall diurnal variation could deepen our understanding of aerosol effects
86 on heavy rainfall. Several previous studies have found that aerosols are related to the changes of the rainfall
87 diurnal variation in other regions (Kim et al., 2010; Gryspeerd et al., 2014b; Fan et al., 2015; Guo et al., 2016;
88 Lee et al., 2016). However, the above studies do not address the change of cloud properties and its sensitivity
89 to different conditions of moisture supply. Although our recent work over BTH region (Zhou et al. 2018)
90 attempted to remove the meteorological effect including circulation and moisture and found that the peak of
91 heavy rainfall shifts earlier on the polluted condition, it only excluded the extreme moisture conditions and
92 focused on aerosol radiative effect on the rainfall diurnal variation. Therefore, this study aims to deepen the
93 previous study (Zhou et al., 2018) through investigating the following questions: (1) how do aerosols
94 (including absorbing aerosols and scattering aerosols) modify the behaviors of the heavy rainfall diurnal
95 variation (start time, peak time, duration and intensity)? And what is the role of moisture in them? (2) how do
96 aerosols influence the associated cloud properties with inclusion of moisture? To solve above questions, we
97 used aerosol optical depth (AOD) as a macro indicator of aerosol pollution and cloud droplet number
98 concentration (CDNC) as a micro indicator of CCN served by aerosols respectively to compare the
99 characteristics of heavy rainfall diurnal variation and associated cloud properties between clean and polluted
100 conditions, and applied aerosol index (AI) to distinguish the different effects of absorbing aerosols and
101 scattering aerosols. In addition, we used the specific humidity (SH) at 850 hPa as an indicator of moisture
102 condition to investigate the possible role of moisture in the relationship between aerosols and rainfall or
103 clouds. The paper is organized as following: The data and methodology are introduced in Sect. 2. Section 3
104 addresses the relationship between aerosol pollution and diurnal variation of heavy rainfall, covering the
105 distinct characteristics of heavy rainfall on clean/polluted condition; the different behaviors of heavy rainfall

106 diurnal variation along with different types of aerosols, and the influence of moisture on the relationship
107 between aerosols and heavy rainfall. Section 4 describes the concurrent changes of cloud properties associated
108 with aerosols and compares the possible influences of CCN (represented by CDNC) and moisture (represented
109 by SH) on the cloud properties. Section 5 gives the hypothesis about the mechanisms of aerosol effects on the
110 heavy rainfall. Discussion and conclusions will be given in Sect. 6.

111

112 **2. Approach**

113 **2.1 Data**

114 Four types of datasets from the year 2002 to 2012 (11 years) are used in this study, which include (1)
115 precipitation, (2) aerosols, (3) clouds, and (4) other meteorological fields.

116 **2.1.1 Precipitation**

117 To study the diurnal variation of heavy rainfall, the gauge-based hourly precipitation datasets are used, which
118 were obtained from the National Meteorological Information Center (NMIC) of the China Meteorological
119 Administration (CMA) (Yu et al., 2007) at 2420 stations in China from 1951 to 2012. The quality control
120 made by CMA/NMIC includes the check for extreme values (the value exceeding the monthly maximum in
121 daily precipitation was rejected), the internal consistency check (wiping off the erroneous records caused by
122 incorrect units, reading, or coding) and spatial consistency check (comparing the time series of hourly
123 precipitation with nearby stations) [Shen et al., 2010]. Here we chose 176 stations in the plain area of BTH
124 region that are below the topography of 100 meter above sea level as shown in Fig.1, because we purposely
125 removed the probable orographic influence on the rainfall diurnal variation, which is consistent with our
126 previous work (Zhou et al., 2018). The record analyzed here is the period of 2002 to 2012. We selected heavy
127 rainfall days when the hourly precipitation amount is more than 8.0 mm/hour (defined by *Atmospheric*
128 *Sciences Thesaurus*, 1994). Here “a day” is counted from 8 LST to 8 LST next day (0 UTC to 24 UTC).

129 **2.1.2 Aerosols**

130 In this study, we used two satellite data and one reanalysis data to investigate the aerosol optical amount and
131 distinguish the different aerosol types.

132 AOD is a proxy for the optical amount of aerosol particles in a column of the atmosphere and serves as the
133 macro indicator for the division of aerosol pollution condition in this study, which was obtained from MODIS
134 (Moderate Resolution Imaging Spectroradiometer) Collection 6 Level-3 aerosol product with the horizontal
135 resolution of $1^{\circ} \times 1^{\circ}$ onboard the Terra satellite (Tao et al., 2015). The quality assurance of marginal or higher
136 confidence is used in this study. The reported uncertainty in MODIS AOD data is on the order of (-0.02-10%),
137 (+0.04+10%) (Levy et al., 2013). The Terra satellite overpass time at the equator is around 10:30 local solar
138 time (LST) in the daytime, and the satellite data is almost missing when it is rainy during the overpass time.

139 As shown in Fig.3, the occurrence of selected heavy rainfall events in this study is mainly later than the
140 satellite overpass time. Therefore, the AOD used here represents the situation of the air quality in advance of
141 heavy rainfall appearance. Many studies have indicated the value of AOD is influenced by moisture condition,
142 which is aerosol humidification effect (Twohy et al., 2009; Altaratz et al., 2013). Hence, we comprehensively
143 analyzed the moisture effect on the rainfall and tried to remove the moisture effect from the relationship
144 between aerosols and rainfall/clouds.

145 The ultraviolet AI from Ozone Monitoring Instrument (OMI) on board the Aura satellite which was
146 launched in July 2004, is used for detecting the different types of aerosols in this study. The OMI ultraviolet
147 AI is a method of detecting absorbing aerosols from satellite measurements in the near-ultraviolet wavelength
148 region (Torres et al., 1998). The positive values of ultraviolet AI are attributed to the absorbing aerosols such
149 as smoke and dust while the negative values of AI stand for the non-absorbing aerosols (scattering aerosols)
150 such as sulfate and sea salt (Tariq and Ali, 2015). The near-zero values of AI occur when clouds and Rayleigh
151 scattering dominate (Hammer et al., 2018). Considering the near-zero values have more uncertainties, we only
152 compare the extreme circumstances of absorbing aerosols and scattering aerosols in this study. The horizontal
153 resolution of AI data is $1^{\circ}\times 1^{\circ}$ and it covers the period of 2005 to 2012.

154 MACC-II (Monitoring Atmospheric Composition and Climate Interim Implementation) reanalysis product
155 produced by ECMWF (the European Centre for Medium-Range Weather Forecasts), provided the AOD
156 datasets for different kinds of aerosols (BC, sulfate, organic matter, mineral dust and sea salt). MACC-II
157 reanalysis products are observationally-based within a model framework, which can offer a more complete
158 temporal and spatial coverage than observation and reduce the shortcomings of simulation that fail in
159 simulating the complexity of real aerosol distributions (Benedetti *et al.*, 2009). The horizontal resolution of
160 MACC-II is also $1^{\circ}\times 1^{\circ}$ with the time interval of six-hour covering the period of 2003 to 2012, and the daily
161 mean values are used in this study in order to be consistent with other datasets.

162 **2.1.3 Clouds**

163 Daily cloud variables, including cloud fraction (CF), cloud top pressure (CTP), cloud optical thickness (COT,
164 liquid and ice), cloud water path (CWP, liquid and ice) and cloud effective radius (CER, liquid and ice), were
165 obtained from MODIS Collection 6 Level-3 cloud product onboard the Terra satellite. The MODIS cloud
166 product combines infrared emission and solar reflectance techniques to determine both physical and radiative
167 cloud properties (Platnick et al., 2017). The validation of cloud top properties in this product has been
168 conducted through comparisons with CALIOP (Cloud-Aerosol Lidar with Orthogonal Polarization) data and
169 other lidar observations (Holz et al., 2008; Menzel et al., 2008), and the validation and quality control of cloud
170 optical products is performed primarily using in situ measurements obtained during field campaigns as well as
171 the MODIS Airborne Simulator instrument (<https://modis-atmos.gsfc.nasa.gov/products/cloud>). Consistent
172 with AOD, the measure of above cloud variables is before the occurrence of heavy rainfall.

173 In addition to the variables in MODIS cloud product, we also calculated CDNC using the joint histogram of
 174 liquid COT and CER from the MODIS Collection 6 Level-3 cloud product. CDNC is retrieved as the proxy
 175 for CCN and also the micro indicator for separating different aerosol conditions in this study. Currently, most
 176 derivations of CDNC assume that the clouds are adiabatic and horizontally homogeneous; CDNC is constant
 177 throughout the cloud's vertical extent, and cloud liquid water content varies linearly with altitude adiabatically
 178 (Min et al., 2012; Bennartz and Rausch, 2017). According to Boers et al. (2006) and Bennartz (2007), we
 179 calculated CDNC (unit: cm^{-3}) through:

$$180 \quad \text{CDNC} = \frac{C_w^{1/2}}{k} \frac{10^{1/2}}{4\pi\rho_w^{1/2}} \frac{\tau^{1/2}}{R_e^{5/2}} \quad (1)$$

181 Where C_w is the moist adiabatic condensate coefficient, and its value depends slightly on the temperature
 182 of the cloud layer, ranging from 1 to $2.5 \times 10^{-3} \text{ gm}^{-4}$ for a temperature between 0 °C and 40 °C (Brennguier,
 183 1991). In this study, we calculated the C_w through the function of the temperature (see Fig.1 in Zhu et al.,
 184 2018) at a given pressure that is 850 hPa. And we have tested the sensitivity of CDNC to the amount of C_w
 185 and found it almost keeps the same when the C_w changes from 1 to $2.5 \times 10^{-3} \text{ gm}^{-4}$. The coefficient k is the
 186 ratio between the volume mean radius and the effective radius, and varies between 0.5 and 1 (Brennguier et al.,
 187 2000). Here we used $k = 1$ for that we cannot get the accurate value of k and the value of k does not influence
 188 the rank of CDNC for the division of aerosol condition in this study. ρ_w is cloud water density. τ and R_e are
 189 the liquid COT and CER with twelve and nine bins respectively in the joint histogram, and we calculated the
 190 CDNC of each bin and get the grid mean CDNC based on the probability distribution of the bin counts from
 191 the joint histogram. To reduce the uncertainty of CDNC retrieval caused by the heterogeneity effect from thin
 192 clouds (Nakajima and King, 1990; Quaas et al., 2008; Grandey and Stier, 2010; Grosvenor et al., 2018), we
 193 selected the CF more than 80%, the liquid COT more than 4 and the liquid CER more than 4 μm when
 194 calculating the CDNC (Quaas et al., 2008).

195 **2.1.4 Other meteorological data**

196 In this study, wind, temperature, pressure and SH data, were obtained from the ERA-Interim reanalysis
 197 datasets with $1^\circ \times 1^\circ$ horizontal resolution and 37 vertical levels at six-hour intervals. The daily mean values of
 198 these variables are used in the study. ERA-Interim is a global atmospheric reanalysis produced by ECMWF,
 199 which covers the period from 1979 to near-real time (Dee et al., 2011).

200

201 **2.2 Methodology**

202 We used both station data of gauge-based precipitation and gridded data including aerosols, clouds and other
 203 meteorological variables. Gridded datasets in this study were downloaded with the horizontal resolution of
 204 $1^\circ \times 1^\circ$, which are consistent with the resolution of MODIS Level-3 products. To unify the datasets, we
 205 interpolated all the gridded datasets onto the selected 176 rainfall stations using the average value in a $1^\circ \times 1^\circ$

206 grid as the background condition of each rainfall station, i.e., the stations in the same $1^{\circ}\times 1^{\circ}$ grid have the same
207 aerosol, cloud and meteorological conditions.

208 **2.2.1 Selection of sub-season and circulation**

209 Consistent with our previous work, we focused on the early summer period (1 June to 20 July) which is before
210 the large-scale rainy season start, in order to remove the large-scale circulation influence and identify the effect
211 of aerosols on local convective precipitation because BTH rainfall during this period is mostly convective
212 rainfall (Yu et al., 2007) with heavy pollution (Zhou et al., 2018). And to unify the background atmospheric
213 circulation, we only selected the rainfall days with southwesterly flow, which is the dominant circulation
214 accounting for 40% of total circulation patterns over the BTH region during early summer (Zhou et al., 2018).

215 **2.2.2 Classification of clean/polluted cases and moisture conditions**

216 With the circulation of southwesterly, we used two indicators to distinguish the clean and polluted conditions
217 from macro and micro perspectives, which are AOD and CDNC. The 25th and 75th percentiles of AOD/CDNC
218 of the whole rainfall days are used as the thresholds of clean and polluted conditions, and the values are
219 shown in Tab.1. There are 514 cases of heavy rainfall on the polluted days and 406 cases of that on the clean
220 days when using AOD, and 805/812 cases on the polluted/clean condition when using CDNC (Fig. 3).

221 The absorbing aerosols are detected using the positive values of AI that is named as absorbing aerosol index
222 (AAI) here, and we can retrieve the scattering aerosol index (SAI) using the negative values of AI. AAI and
223 SAI are also divided into two groups using the threshold of 25th/75th percentile as shown in Tab.1. We used
224 AAI/SAI more than 75th percentile as the extreme circumstances of absorbing/scattering aerosols to compare
225 their impacts on the heavy rainfall. The sample numbers are 375 and 550 respectively for the extreme AAI
226 and SAI cases. Using the same method, we chose cases with more BC/sulfate when the AOD of BC/sulfate is
227 larger than the 75th percentile of itself in all rainy days, and cases with less BC/sulfate when that is less than
228 the 25th percentile of itself in the same situation. Accordingly, we selected 459 heavy rainfall cases with more
229 BC and 274 cases with less BC. Similarly, 361 cases with more sulfate and 419 cases with less sulfate were
230 selected (Fig. 6).

231 The SH at 850 hPa is used as the indicator of moisture condition under the cloud base. We chose wet cases
232 when the SH on that day is larger than 75th percentile of the whole rainy days, and chose dry cases when SH
233 on that day is less than the 25th percentile of the whole rainy days (the thresholds are shown in Tab. 1).

234 **2.2.3 Statistical analysis**

235 We adopted the probability distribution function (PDF) to compare the features of heavy rainfall and cloud
236 variables on different conditions of aerosols, through which we can understand the changes of rainfall/cloud
237 properties more comprehensively. The numbers of bins we selected in the study have been all tested for better
238 representing the PDF distribution. Student's t-test is used to examine the statistical significance level of the

239 differences or correlations between the different groups variables.

240

241 **3. Changes of heavy rainfall**

242 In this study, we applied two indicators (AOD and CDNC) to identify the aerosol pollution. AOD is usually
243 used as the macro indicator of aerosol pollution, which represents the optical feature of aerosol particles rather
244 than the micro CCN (Shinozuka et al., 2015). To better identify the aerosol-cloud interaction, we intentionally
245 applied the CDNC as the indicator of CCN (Zeng et al., 2014; Zhu et al., 2018).

246 We first investigated the value distribution of AOD and CDNC over the BTH region. Figure 2a&b shows
247 the PDFs of AOD and CDNC on the non-rainfall days, rainfall days and heavy rainfall days respectively. We
248 found that the ranges of AOD values under the above three conditions are almost similar that is between 0-5
249 and their probability peaks all occur at around 1.2 (Fig. 2a). In contrast, CDNC shows different ranges among
250 the three conditions, which ranges from around 30 cm⁻³ to 600 cm⁻³ on the rainfall days and heavy rainfall
251 days while from around 50 cm⁻³ to 800 cm⁻³ on the non-rainfall days. Besides, the proportion of low CDNC is
252 relatively high on the non-rainfall days (Fig. 2b). Accordingly, the range of AOD remains similar while the
253 range of CDNC is shortened on the rainfall days, probably because the cloud droplets become larger on
254 rainfall days, which could cause the reduction of number concentration. Therefore, to obtain comparable
255 samples, we use percentile method to select respective clean and polluted cases based on above two indicators
256 in order to better compare the characteristics of heavy rainfall. Hence the heavier pollution corresponds to
257 larger optical amount of aerosols measured by AOD, and more amount of aerosols that could serve as CCN
258 measured by CDNC.

259 **3.1 Characteristics**

260 Our previous study (Zhou et al. 2018) has reported the distinct peak shifts of rainfall diurnal variation between
261 clean and polluted days using the indicator of AOD over the BTH region during early summer. Similar with
262 our previous study, the PDF of the heavy rainfall peak time shows that the maximum of rainfall peak is about
263 two hours earlier on the polluted days (20:00 LST) than that on the clean days (22:00 LST) (Fig. 3a). To
264 comprehensively recognize the changes of rainfall diurnal variation associated with air qualities, here we
265 examined the PDF of the start time, the duration and the intensity besides the peak time of heavy rainfall.

266 As shown in Fig. 3a, the start time of heavy rainfall exhibits a significant advance on the polluted days. The
267 secondary peak on the early morning is ignored here because the early-morning rainfall is usually associated
268 with the mountain winds (Wolyn et al., 1994; Li et al., 2016) and the nighttime low-level jet (Higgins et al., 1997;
269 Liu et al., 2012) that is beyond the scope of this study. The time for the maximum frequency of heavy rainfall
270 initiation is around 6 hours earlier on the polluted days, shifting from around 0:00 LST on the clean days to
271 the 18:00 LST (Fig. 3a). Regarding the rainfall durations, the average persistence of heavy rainfall on polluted
272 days is 0.8 hours longer than that on clean days (Tab. 2). According to the PDF shown as in Fig. 3a, the

273 occurrence of short-term precipitation (≤ 6 hours, Yuan et al., 2010) decreases while that of long-term
274 precipitation (> 6 hours, Yuan et al., 2010) increases. The intensity of hourly rainfall exhibits a non-significant
275 increase on the polluted days.

276 The distinct behaviors of heavy rainfall diurnal variation between clean and polluted days have been well
277 demonstrated using the indicator of AOD. Using CDNC as the indicator of CCN, the above-mentioned results
278 are also significant, as shown in Fig. 3b. The start time and peak time of heavy rainfall on the polluted
279 condition also show significant advances compared with that on the clean condition, with the average
280 advances of 2.2 hours and 2.6 hours respectively (Tab. 2). The duration of heavy rainfall on the polluted
281 condition is also prolonged, which is 0.5 hours longer in average (Tab. 2). Similar with the results based on
282 AOD, the difference of rainfall intensity between clean and polluted conditions using CDNC does not pass the
283 95% statistical confidence level as well.

284 Hence, the results using either AOD or CDNC show that the start and peak time of heavy rainfall occur
285 earlier and the duration becomes longer under pollution. We found the AOD and CDNC only have a
286 non-significant positive correlation, which denotes that the selected cases could be different between using
287 AOD and CDNC. The differences between the two indicators might be attributed to the non-linear relationship
288 between CCN and aerosol pollution (e.g., Jiang et al., 2016), the misdetection of AOD when the humidity is
289 high (Boucher and Quaas, 2012), the calculation uncertainty of CDNC, and the sampling differences between
290 AOD and CDNC. Since the two indicators represent aerosols from the different perspectives, we cannot
291 identify which one is more reliable. Because the change of rainfall intensity is not significant based on either
292 AOD or CDNC, the following analysis only focuses on studying the changes of start time, peak time and
293 duration of heavy rainfall along with aerosol pollution.

294 **3.2 Sensitivities to aerosol types**

295 Using the indicator of AI, we further investigated the distinct behaviors of heavy rainfall diurnal variation
296 related to absorbing aerosols and scattering aerosols respectively. The PDF of start time, peak time and
297 duration of heavy rainfall under the extreme circumstances of absorbing aerosols and scattering aerosols are
298 compared in Fig. 4. Here, we briefly named the days with extreme large amount of absorbing aerosols as
299 absorbing aerosol days and with more scattering aerosols as scattering aerosol days. The start time of heavy
300 rainfall on absorbing aerosol days shows a significant earlier compared with that on scattering aerosol days
301 (Fig. 4a), with 0.7 hours advance in average (Tab. 3). Similarly, the rainfall peak time also shows earlier on
302 absorbing aerosol days (Fig. 4b), with an average advance of 1.6 hours (Tab. 3). The rainfall duration on
303 scattering aerosol days shows longer than that on absorbing aerosol days, which are 6.0 hours and 5.0 hours
304 respectively in average (Tab. 3). All the above-mentioned differences between the two groups have passed 95%
305 statistical confidence level. The results indicate that the absorbing aerosols and scattering aerosols may have
306 different or inverse effects on the heavy rainfall that absorbing aerosols may generate the heavy rainfall in
307 advance while the scattering aerosols may delay and prolong the heavy rainfall.

308 To further verify the different behaviors of heavy rainfall diurnal variation associated with two different
309 types of aerosols, we purposely re-examine the above-mentioned phenomena using BC/sulfate that can
310 represent typical absorbing/scattering aerosols over the BTH region. BC has its maximum center over BTH
311 region (Fig. 5a) and our previous study has indicated that the radiative effect of BC low-level warming may
312 facilitate the convective rainfall generation (Zhou et al., 2018). The percentage of sulfate is also large over the
313 BTH region (Fig. 5b) and sulfate is one of the most effective CCN that influences the precipitation in this
314 region (Gunthe et al., 2011). Accordingly, we selected the cases with different amounts of BC and sulfate
315 AOD to compare their roles on the diurnal variation of heavy rainfall. The methods have been described in
316 Sect. 2.2.2. The PDF of the start time, peak time and duration of heavy rainfall in the cases with more/less
317 amount of BC are shown in Fig. 6a, respectively. The most striking result is that the maximum frequency of
318 rainfall start time in the more BC cases evidently shifts earlier (Fig. 6a). Meanwhile, the mean peak time in
319 the more BC cases shows 1.1 hour earlier than that in the less BC cases (Tab. 3). And the duration of heavy
320 rainfall is slightly shortened by the averaged 0.2 hours in the more BC cases. The features in more BC cases
321 are consistent with the above results of absorbing aerosols. In contrast, when the sulfate has larger amount, the
322 mean start time of rainfall is delayed by 0.5 hours, while the duration shows a significant increase by 1.5
323 hours in average (Tab. 3). The behaviors in the more sulfate cases also exhibit similar with the above results
324 of scattering aerosols, except for the peak time that shows later in the scattering aerosol cases but a little
325 earlier in the more sulfate cases (Tab. 3).

326 **3.3 Influence of moisture**

327 Moisture supply is an indispensable factor for the precipitation formation, and it also has an important impact
328 on AOD (Boucher and Quaas, 2012). Since the southwesterly circulation can not only transport pollutants but
329 also plenty of moisture to the BTH region (Wu et al., 2017), more pollution usually corresponds to more
330 moisture for the BTH region (Sun et al., 2015) so that it is hard to completely remove the moisture effect on
331 the above results in a pure observational study. Here we attempt to recognize the moisture effect on the heavy
332 rainfall to further understand the above aerosol-associated changes. Because the moisture supply for BTH is
333 mainly transported via low-level southwesterly circulation, we purposely used the SH at 850 hPa as the
334 indicator of moisture condition.

335 Using the similar percentile method with polluted/clean days, we compared the heavy rainfall
336 characteristics in the more humid (more than 75th percentile) and the less humid (less than 25th percentile)
337 environments regardless of the aerosol condition, as shown in Fig. 7a. The results show that the start time of
338 heavy rainfall is delayed by 0.9 hours, the peak time is 0.6 hours earlier and the duration is prolonged by 2.0
339 hours in average in the more humid environment, which is similar with the results of the more sulfate cases.
340 Besides, the same results are obtained using different moisture indicator, e.g. the 850 hPa absolute humidity.
341 These results indicate the advance of heavy rainfall start time on the polluted days is not caused by more
342 moisture supply, while the longer duration and earlier peak in the more sulfate cases might be related to the

343 increased moisture supply. To further identify the role of sulfate, we examined the sensitivities of the results
344 associated with sulfate under different moisture condition. In the dry (SH less than 25th percentile) and
345 intermediate cases (SH between 25th - 75th percentiles), the heavy rainfall still shows later start time, earlier
346 peak and significant longer duration with the increase of sulfate, while the change of peak time is not
347 significant in the dry cases; in the high moisture cases (SH more than 75th percentile), it shows earlier peak
348 and shorter duration in the more sulfate cases while the change of start time is not significant. Therefore, we
349 suppose that the impact of sulfate aerosols on the heavy rainfall is sensitive to moisture, and notably the
350 sulfate could contribute to the longer duration in the polluted cases when it is relatively dry.

351 We also investigate the distributions of moisture and rainfall behaviors in the clean and polluted cases
352 respectively using AOD and CDNC (Fig. 7 b&c). The results show that the relationship between moisture and
353 rainfall start time/peak time/duration is not linear. The distribution of SH exhibits a slight increase with
354 pollution in the AOD cases, indicating that the polluted cases selected by AOD are accompanied with more
355 moisture than the clean cases. However, when fixing the moisture at a certain range especially at the relative
356 dry condition (for example, the SH between 8-12 g/kg), we can detect the similar phenomena of earlier
357 start/peak time and longer duration in the polluted cases based on either AOD or CDNC. To further clarify the
358 characteristics of heavy rainfall associated with pollution, we removed the samples with high SH (SH more
359 than 75th percentile) and found that the results in section 3.1 remain, that is the start/peak time of heavy
360 rainfall is in advance and the duration is prolonged with the increase of AOD/CDNC when SH is less than
361 12.95 g/kg (75th percentile) (Fig. 8).

362 The above results indicate that the advance of heavy rainfall start in the polluted cases is independent of
363 moisture condition, while the advance of peak time and longer duration could be influenced by the moisture
364 effect. For the earlier peak time of heavy rainfall, we suppose the role of BC (absorbing aerosols) might be
365 dominant because the change of peak time in the former analysis is more significant (Tab. 3) although the
366 sulfate and moisture also have positive contribution. The increased sulfate (scattering aerosols) contributes to
367 the longer duration of heavy rainfall (Fig. 6b), but the role of sulfate is kind of sensitive to the moisture
368 condition. With the increase of sulfate, the duration is longer when the moisture condition is relatively dry
369 while becomes shorter when it is extremely wet. Overall, when removing the extremely high moisture cases,
370 the earlier start/peak time and longer duration of heavy rainfall associated with aerosol pollution are
371 significant.

372

373 **4. Changes of clouds**

374 To understand the cloud effect of aerosols during heavy rainfall diurnal variation, we need to recognize the
375 associated cloud characteristics on the clean and polluted conditions. The cloud properties we used were
376 obtained from satellite product that was measured at the same time with aerosols before the occurrence of

377 heavy rainfall. The differences of cloud features were examined in both macroscopic (including CF, CTP,
378 COT and CWP) and microscopic properties (including CER) on the clean and polluted conditions based on
379 AOD and CDNC respectively.

380 **4.1 Characteristics**

381 Using AOD as the macro aerosol indicator, as shown in Fig. 9, the PDF distribution shows that the CF on the
382 polluted condition is evidently larger than that on the clean condition. The average CF is 62.8% on the clean
383 condition, and 89.3% on the polluted condition (Tab. 4). The average CTP on the polluted condition is 487.3
384 hPa, which is larger than 442.3 hPa on the clean condition, indicating that the cloud top height is lower on the
385 polluted days. The COT, CWP and CER were further analyzed for the liquid and ice portions of clouds as
386 shown in Fig. 9. Both liquid and ice COT on the polluted condition exhibit significant increases compared
387 with that on the clean condition. The mean amount of liquid COT is increased by 3.1 and ice COT increases
388 by 6.2 (Tab. 4). Similar with COT, the amounts of liquid and ice CWP also increase under pollution, which
389 increase by 33.6 g/m² and 88.2 g/m² respectively. In addition, the liquid CER is increased by 0.8 μm and the
390 ice CER is decreased by 2.8 μm on the polluted days. The differences of above cloud properties between clean
391 and polluted cases have all passed the 95% statistical confidence level.

392 Using CDNC as the micro aerosol indicator, the above-mentioned changes of cloud properties are
393 consistent with that using AOD, except for liquid CER (Fig. 9). Since the calculation method of CDNC is not
394 independent on the liquid COT and liquid CER, we would not directly compare the results of liquid COT and
395 CER based on CDNC with those based on AOD here. But according to other variables that are independent of
396 the CDNC calculation, we found the cases with more CDNC are accompanied with the increase of CTP, ice
397 COT and liquid & ice CWP, which increase by 90.2 hPa, 24.4, 112.4 g/m² and 224.1 g/m² respectively (Tab. 4)
398 and all of which are consistent with the results based on AOD. The CER of ice clouds also shows a consistent
399 decrease by 9.5 μm on the polluted condition based on CDNC. We noticed that the changes of
400 COT/CWP/CER for both liquid and ice based on CDNC are much larger than that based on AOD, which
401 indicates that these cloud properties might be more sensitive to the indicator of CDNC rather than AOD.

402 According to the above comparison, the concurrent changes of cloud properties along with heavy rainfall
403 diurnal variation show consistent results using the two aerosol indicators (AOD and CDNC). The pollution
404 corresponds to the increase of CF, ice COT, liquid and ice CWP, but the decrease of cloud top height (the
405 increase of CTP corresponds to the decrease of cloud top height) and ice CER. The liquid COT and liquid
406 CER are also increased with the enhanced pollution in the AOD analysis. Besides, the above-mentioned
407 results exhibit significant when we limited the moisture to the dryer condition (SH less than 25th percentile) or
408 intermediate condition (SH between 25th - 75th percentile). When the moisture is higher (SH more than 75th
409 percentile), the change of CTP become not significant based on CDNC.

410 According to these results, we made the following speculation: First, the CF, liquid & ice COT and CWP

411 increase with pollution, because the aerosols serving as CCN can nucleate a larger number of cloud droplets
412 which in a moisture sufficient environment can hold more liquid water in the cloud. Second, the CTP
413 increases (the cloud top height decreases) under pollution using both AOD and CDNC, because the earlier
414 start of the precipitation process (Fig. 3) inhibits the vertical growth of clouds. Third, the ice CER decreases
415 under pollution using either AOD or CDNC, because the increased cloud droplet number leads to more cloud
416 droplets transforming into ice crystals and causes the decrease of ice CER (Chylek et al., 2006; Zhao et al.,
417 2018; Gryspeerd et al., 2018). However, the results of liquid CER might have uncertainties. The liquid CER
418 is increased when AOD increases (Fig. 9), which might be related to the aerosol humidification effect, the
419 misdetection of AOD and cloud water, and the earlier formation of the clouds and precipitation on the polluted
420 days. Since we cannot distinguish the liquid part of mix-phased clouds from liquid (warm) clouds in the
421 observation, the above-mentioned change of liquid cloud properties might come from that of both the liquid
422 (warm) clouds and the liquid part of mixed-phase clouds. Likewise, the above-mentioned change of ice cloud
423 properties might come from that of both ice (cold) clouds and the ice part of mixed-phase clouds. Currently
424 the physical processes of cold clouds and mixed-phase clouds have been not clarified yet, including the
425 diffusional growth, accretion, riming and melting process of ice precipitation (Cheng et al., 2010), which
426 needs numerical model simulations to be further explored.

427 **4.2 Sensitivities to CCN (represented by CDNC) and moisture**

428 Section 3.3 has shown that the diurnal variation of heavy rainfall with more moisture supply is similar with
429 the changes of heavy rainfall with more sulfate aerosols. We assume that the moisture under the cloud base
430 and the sulfate serving as CCN both influence the cloud properties (Yuan et al., 2008; Jiang et al., 2008; Jung
431 et al., 2013; Qiu et al., 2017). To identify the effect of CCN on clouds and its sensitivity to moisture, using
432 CDNC to represent CCN, we purposely investigated the changes of above cloud properties on the different
433 conditions of the CDNC and the low-level moisture (850hPa SH) respectively.

434 We categorized all cases of heavy rainfall into four groups, which are (1) clean and dry, (2) polluted and
435 dry, (3) clean and wet, (4) polluted and wet, and checked the changes of above cloud properties, as shown in
436 Tab. 5. To retrieve the comparable samples, here “clean/polluted” refers to the CDNC on that day less/more
437 than 25th/75th percentile of the CDNC among the heavy rainfall days, and similarly, the “dry/wet” refers to the
438 SH on that day less/more than 25th/75th percentile of itself among the heavy rainfall days. The average CDNC
439 is 125.54 cm⁻³ on the dry condition and 120.71 cm⁻³ on the wet condition, and the average SH is 11.62 g/kg
440 and 11.73 g/kg on the clean and polluted conditions respectively, thus we consider the CDNC or SH remain
441 almost the same when the other condition changes. We tested the significance of differences between group 1
442 and 2, group 1 and 3, group 2 and 4, group 3 and 4. Because the CF is fixed above 80% when calculating the
443 CDNC (see in Sect. 2.1.3), here the selected groups all belong to the condition of higher CF.

444 Comparing the results of group 1 and 2, which are both on the dry condition, we can identify the influence
445 of CDNC on the cloud properties, which represents the effect of CCN. The changes of these cloud variables

446 are the same as that in Sect. 4.1, that the CF, ice COT and liquid & ice CWP are increased on the polluted
447 condition, while the cloud top height and ice CER are decreased based on CDNC. Among these variables, the
448 ice COT and liquid & ice CWP are especially larger on the polluted condition, which are 3-4 times larger than
449 that on the clean condition (Tab. 5). On the wet condition, comparing the group 3 and 4, the changes are
450 similar that the CF, ice COT and liquid & ice CWP are increased and the ice CER are decreased but the
451 change of CTP becomes not significant. However, the changes of these variables on the dry condition are
452 evidently enhanced than that on the wet condition, which indicates these cloud properties might be more
453 sensitive to CDNC on the dry condition. The above comparisons indicate that with the increase of CDNC
454 (CCN), the CF, ice COT and liquid & ice CWP are increased while the ice CER is decreased regardless of the
455 moisture amount.

456 Comparing the results of group 1 and 3, we can get the changes of cloud properties related only to moisture
457 on the same clean condition. A common feature is that CF, CTP, COT and CWP both for liquid and ice exhibit
458 increases along with the increase of moisture. Compared with the CTP on the clean and dry condition, it
459 increases on both polluted & dry condition (group 2) and clean & wet condition (group 3), but on the former
460 condition its increase is larger, which indicates the influence of moisture on CTP might be secondary
461 compared to the CDNC (CCN) effect. Similarly, comparing the COT/CWP in group 2 and 3, the increases of
462 COT and CWP both for liquid and ice in group 2 are much larger than that in group 3, which indicates that the
463 influences of moisture on COT and CWP may not overcome the influence of CCN. With the increase of
464 moisture, the change of liquid CER is not significant on the same clean condition, but the ice CER is
465 significantly decreased. On the polluted condition, comparing group 2 and 4, we found the COT and CWP
466 both for liquid and ice on the wet condition are evidently smaller than that on the dry condition, which
467 indicates that increasing the moisture might partly compensate for the influence of CDNC (CCN) on
468 COT/CWP. Besides, the liquid CER exhibits a slight increase with increased moisture in the same polluted
469 environment, which may further support the idea that the increased CCN could nucleate more cloud water
470 with increased moisture.

471 The results above indicate that both CDNC (CCN) and moisture have impacts on cloud properties. They
472 both contribute to the increase of CF, CTP, COT and CWP, in which the influence of CDNC (CCN) on COT
473 and CWP are significantly larger than moisture. Both CDNC and moisture correspond to the significant
474 decrease of ice CER, while only CDNC corresponds to the decrease of liquid CER and that might be ascribed
475 to the calculation method of CDNC. To reduce uncertainties, we have tested the SH at different levels (e.g.,
476 700 hPa and 800 hPa) and different moisture indicator (e.g. absolute humidity) to verify these results, and
477 found most cloud variables show the similar changes with above except for the CTP and the liquid CER,
478 which indicates the changes of CTP and liquid CER are more sensitive and have larger uncertainties. Since
479 the behaviors of cloud changes are similar along with the increase of either CDNC (CCN) or moisture but
480 more sensitive to the former, the results in Sect. 4.1 might actually reflect the combined effect of CCN and
481 moisture, and the aerosol (CCN) effect on these cloud properties might be dominant on the polluted days.

482 Therefore, considering the results from this subsection and Sect. 3.3 that the changes of cloud features
483 become smaller in the higher moisture environment than that in the dryer environment and the duration of
484 heavy rainfall is relatively shortened with pollution when it is extremely wet (Sect. 3.3), we speculate that the
485 sulfate (CCN) effect might be suppressed in a relatively wet environment. Due to the limitations of
486 observational study, we currently cannot figure out the respective roles of aerosols and moisture.

487

488 **5. Hypothesis**

489 According to all the above results, we have made hypotheses about the aerosol effects on the heavy rainfall
490 over the BTH region. In Sect. 3.1 we found that the heavy rainfall has earlier start and peak time, and longer
491 duration on the polluted condition. And afterwards, the earlier start of rainfall under pollution was found
492 related to absorbing aerosols mainly referring to BC (Fig. 4a&6a). We also compared the effect of BC on the
493 associated clouds. Figure 10a shows the CF larger than 90% rarely occurs in the more BC environment, which
494 might be associated with the semi-direct effect of BC (Ackerman, 2000) or estimated inversion strength and
495 BC co-vary. This result indicates the influence of BC on the heavy rainfall in Fig. 6a is mainly due to the
496 radiative effect rather than the cloud effect. The mechanism of BC effect on the heavy rainfall can be
497 interpreted by our previous study (Zhou et al., 2018) as: BC absorbs shortwave radiation during the daytime
498 and warms the lower troposphere at around 850 hPa, and then increases the instability of the lower to middle
499 atmosphere (850-500 hPa) so that enhances the local upward motion and moisture convergence. As a result,
500 the BC-induced thermodynamic instability of the atmosphere triggers the occurrence of heavy rainfall in
501 advance. Thus, the low-level heating effect of BC might play a dominant role in the beginning of rainfall
502 especially before the formation of clouds during the daytime.

503 The delayed start of heavy rainfall with scattering aerosols in Fig. 4a and more sulfate in Fig. 6b is
504 consistent with many studies that both the radiative effect and cloud effect of sulfate-like aerosols could delay
505 or suppress the occurrence of rainfall (Guo et al., 2013; Wang et al., 2016; Rosenfeld et al. 2014). Sulfate-like
506 aerosols as scattering aerosols could prevent the shortwave radiation from arriving at the surface thus cool the
507 surface and stabilize the atmosphere, which suppresses the rainfall formation (Guo et al., 2013; Wang et al.,
508 2016). Sulfate-like aerosols serving as CCN can also suppress the rainfall by cloud effect through reducing the
509 cloud droplet size and thus suppressing the collision-coalescence process of cloud droplets (Albrecht 1989;
510 Rosenfeld et al. 2014). Figure 10b does shows that in contrast with BC, the CF larger than 90% is
511 significantly increased in the more sulfate environment, which indicates the sulfate-like aerosols might have
512 more evident influence on the clouds and subsequently the rainfall changes associated with sulfate are
513 probably due to the cloud effects. Another significant feature is the longer duration of heavy rainfall in the
514 scattering aerosol cases, more sulfate cases and high moisture cases (Fig 4c, 6b&7a). We speculate that the
515 longer duration is caused by both the cloud effect of sulfate-like aerosols and the increased moisture supply,
516 because increasing either CCN or the moisture supply can increase cloud water (Sect. 4.2), which could lead

517 to the longer rainfall duration. To further investigate the mechanism of longer duration, we need the assistance
518 of numerical model simulations in the future work.

519 Accordingly, we speculate that the earlier start time of heavy rainfall related to absorbing aerosols (BC) is
520 due to the radiative heating of absorbing aerosols, while the longer rainfall duration is probably caused by
521 both the cloud effect of sulfate-like aerosols and the increased moisture supply. As a summary we use a
522 schematic diagram (Fig. 11) to illustrate how aerosols modify the heavy rainfall in the meteorological
523 background of southwesterly over the BTH region. On one hand, BC heats the lower troposphere, changing
524 the thermodynamic condition of atmosphere, which increases the upward motion and accelerates the
525 formation of clouds and rainfall. On the other hand, the increased upward motion transports more sulfate-like
526 particles and moisture into the clouds so that the increased aerosols serving as CCN could nucleate more cloud
527 water, thus prolong the duration of rainfall. As a result, the earlier start and peak time, and longer duration of
528 heavy rainfall over BTH region might due to the combined effect of aerosol radiative effect, aerosol cloud
529 effect. To further verify the individual effect, we need to conduct numerical model simulations in our future
530 study.

531

532 **6. Discussion and conclusions**

533 **6.1 Discussion**

534 In this study we used two aerosol indicators, AOD and CDNC, which discriminates the pollution levels for
535 different purposes. AOD is a good proxy for the large-scale pollution level, but it stands for the optical feature
536 of aerosols and cannot well represent CCN when we focused on the aerosol-cloud interaction (Shinozuka et al.,
537 2015). CDNC is a better proxy for CCN compared with AOD, which facilitates the study on the cloud changes
538 associated with aerosol pollution. But the retrieved CDNC has larger uncertainties. First, the assumptions in
539 the calculation of CDNC are idealized that CDNC is constant with height in a cloud and cloud liquid water
540 increases monotonically at an adiabatic environment (Grosvenor et al., 2018), but the target of this study is the
541 convective clouds with rainfall that may be not consistent with the adiabatic assumption. Second, as indicated
542 by Grosvenor et al. (2018), the uncertainties in the pixel-level retrievals of CDNC from MODIS with $1^\circ \times 1^\circ$
543 spatial resolution can be above 54%, which come from the uncertainties of parameters and the original COT
544 and CER data using in the calculation, and also the influence of heterogeneity effect from thin clouds. To
545 reduce the influence of heterogeneity effect as much as possible, we have attempted to limit the conditions of
546 CF, liquid COT and CER when calculating CDNC in the study. Besides, this study primarily focuses on the
547 relative changes of CDNC, which may be also influenced by the potential systematic biases in the CDNC
548 calculation, but actually reduced the uncertainties of absolute values. Another problem about CDNC in this
549 study is that the CDNC could be influenced by updraft velocity because both increased CCN and updraft
550 velocity could enhance aerosol activation and increase CDNC (Reutter et al., 2009). Since we cannot get any

551 in-cloud long-term updraft data, we used the vertical velocity at 850 hPa obtained from ERA-interim
552 reanalysis data to roughly represent the cloud base updraft and investigated the possible relationship between
553 CDNC and updraft. The results show that there is no significant correlation between CDNC and vertical
554 velocity, although the updraft is relatively intensified in the polluted cases. We also examined the change of
555 rainfall based on CDNC under three certain ranges of vertical velocity (less than 25th percentile, between 25th
556 -75th percentile and more than 75th percentile), and found the primary results are similar.

557 In addition to AOD and CDNC, we also applied ultraviolet AI and AOD of BC/sulfate to identify different
558 types of aerosols. We found that the AI has a weak positive correlation with AOD from MODIS, which
559 indicates the results on absorbing aerosol days might represent the results on polluted days if identified by
560 AOD. To avoid the uncertainty, we re-examined the results using AI when removing the polluted cases
561 identified by AOD, and found the major results remain. The comparisons of BC/sulfate AOD cases also have
562 uncertainties because they are retrieved from MACC reanalysis data. Although the above four indicators have
563 their own uncertainties, currently we cannot find more reliable datasets in a long-term observational record.
564 The major findings using these four indices could well identify the changes of rainfall and clouds
565 accompanied with aerosols, but are insufficient to clarify the aerosol effect on clouds and precipitation.

566 This study has clearly identified the relationship of the aerosol pollution and the diurnal changes of heavy
567 rainfall and associated clouds in the BTH region. However, although this work has attempted to exclude the
568 impacts from the meteorological background particularly circulation and moisture, the observation study still
569 has its limitations on studying aerosol effects on rainfall and clouds: first, the observational datasets have their
570 noise and uncertainty, including the misdetection of CF in the satellite product when AOD is large (Brennan et
571 al., 2005; Levy et al., 2013) and the mutual interference between liquid and ice clouds (Holz et al., 2008;
572 Platnick et al., 2017); Second, the meteorological co-variations cannot be completely removed thus bring the
573 uncertainties of the results, e.g., the meteorology might affect the relationship between AOD and CF (Quaas et
574 al., 2010; Grandey et al., 2013) and the relationship between AOD and CTP (Gryspeerd et al., 2014a); Third,
575 the different types of aerosols cannot be completely well separated, although we used AI index and AOD of
576 BC/sulfate to identify the respective effects of absorbing aerosols and scattering aerosols. In addition, we
577 selected the extreme ranges of AOD/CDNC to compare the characteristics of heavy rainfall and associated
578 clouds, which could bring such uncertainties that these extreme conditions might be related with distinct
579 microphysical process or meteorological background. We further examined the results using the middle range
580 of AOD and CDNC such as 25th – 50th percentile versus 50th -75th percentile. The results are basically the same
581 except that the peak time change is not significant based on AOD. Numerical model simulations are
582 necessarily applied to further study the specific impact of aerosols on the heavy rainfall. And the detailed
583 processes of aerosol effect on the precipitation formation of mix-phased and cold clouds also needs further
584 exploration in our future study.

585 **6.2 Conclusions**

586 Using the gauge-based hourly rainfall records, aerosol and cloud satellite products and high temporal
587 resolution reanalysis datasets during 2002-2012, this study investigated the different characteristics of heavy
588 rainfall in the diurnal time scale on the clean and polluted conditions respectively. Based on the macro and
589 micro aerosol indicators including AOD from MODIS aerosol product and calculated CDNC from MODIS
590 cloud product, three significant features of heavy rainfall diurnal change associated with aerosols are found,
591 that is the rainfall start and peak time occur earlier and the duration becomes longer under pollution.

592 The different relationships of absorbing and scattering aerosols with the heavy rainfall diurnal shift were
593 distinguishable using ultraviolet AI from OMI and reanalysis AOD of two aerosol types (BC and sulfate). The
594 absorbing aerosols (BC) correspond to the earlier start and peak time of heavy rainfall, while the scattering
595 aerosols (sulfate) correspond to the delayed start time and the longer duration. Considering the plausible effect
596 of moisture, further analysis indicates the duration of heavy rainfall is prolonged in the presence of more
597 sulfate on the relatively dry condition but is shortened on the extremely wet condition.

598 By comparing the characteristics of cloud macrophysics and microphysics variables, using both AOD and
599 CDNC we found the CF, ice COT, liquid and ice CWP are increased on the polluted condition, but the cloud
600 top height and the ice CER are reduced. Liquid COT and liquid CER are also increased in AOD analysis.
601 Comparing the influences of CDNC which represents CCN and SH at 850 hPa which represents moisture
602 condition respectively on these cloud variables, the cloud properties show similar changes with the increase of
603 CDNC and moisture, but seem more sensitive to the CDNC (CCN), e.g., the liquid & ice COT and CWP are
604 increased more significantly in high CDNC than in high SH.

605 According to these results, we speculate that both aerosol radiative effect and cloud effect have impacts on
606 the diurnal variation of heavy rainfall in the BTH region. The heating effect of absorbing aerosols especially
607 BC increases the instability of the lower to middle atmosphere so that generates the heavy rainfall occurrence
608 in advance. And the increased moisture supply and increased aerosols which could nucleate more cloud water
609 in the cloud, leading to the longer duration of heavy rainfall.

610

611 **Data availability**

612 We are grateful to the National Meteorological Information Centre (NMIC) of the China Meteorological
613 Administration (CMA) for providing hourly precipitation datasets. MODIS aerosol and cloud data were
614 obtained from <http://ladsweb.modaps.eosdis.nasa.gov>; ultraviolet AI data from OMI was obtained from
615 <https://daac.gsfc.nasa.gov/datasets?keywords=OMI&page=1>; MACC-II and ERA-interim reanalysis datasets
616 were obtained from <http://apps.ecmwf.int/datasets>.

617 **Author contributions**

618 JY and SZ conceived the study. SZ processed data and drew the figures. SZ and JY analyzed the observational

619 results and WCW, CZ and DG gave the professional guidance. PS provided the hourly precipitation dataset.
620 SZ and JY prepared the manuscript with contributions from WCW and CZ.

621 **Competing interests**

622 The authors declare that they have no conflict of interest.

623 **Acknowledgements**

624 Jing Yang, Daoyi Gong & Peijun Shi are supported by funds from the National Natural Science Foundation of
625 China (41775071 and 41621061) and the National Key Research and Development Program-Global Change
626 and Mitigation Project: Global Change Risk of Population and Economic System: Mechanism and
627 Assessment (2016YFA0602401 and 2018YFC1505903), Siyuan Zhou is supported by funds from State Key
628 Laboratory of Earth Surface Processes and Resource Ecology and Key Laboratory of Environmental Change
629 and Natural Disaster. Wei-Chyung Wang acknowledges the support of grants (to SUNYA) from the Office of
630 Sciences (BER), U.S. DOE and the U.S. National Science Foundation (1545917) in support of the Partnership
631 for International Research and Education project at the University at Albany. We deeply appreciate two
632 anonymous referees for their in-depth comments and constructive suggestions.

633

634 **References:**

- 635 Ackerman, A. S.: Reduction of Tropical Cloudiness by Soot, *Science*, 288, 1042-1047,
636 doi:10.1126/science.288.5468.1042, 2000.
- 637 Albrecht, B. A.: Aerosols, cloud microphysics, and fractional cloudiness, *Science*, 245, 1227-1230,
638 doi:10.1126/science.245.4923.1227, 1989.
- 639 Altaratz, O., Bar-Or, R. Z., Wollner, U., and Koren, I.: Relative humidity and its effect on aerosol optical
640 depth in the vicinity of convective clouds, *Environ. Res. Lett.*, 8, 034025,
641 doi:10.1088/1748-9326/8/3/034025, 2013.
- 642 Anonymous: Atmospheric Sciences Thesaurus, China Meteorological Press: Beijing, China, 1994. (in
643 Chinese)
- 644 Anonymous: IPCC fifth assessment report, *Weather*, 68, 310-310, 2013.
- 645 Bellouin, N., Quaas, J., Morcrette J. -J., and Boucher, O.: Estimates of aerosol radiative forcing from the
646 MACC re-analysis, *Atmos. Chem. Phys.*, 13, 2045-2062, doi:10.5194/acp-13-2045-2013, 2013.
- 647 Benedetti, A., Morcrette, J. J., Boucher, O., Dethof, A., Engelen, R. J., Fisher, M., Flentje, H., Huneeus, N.,
648 Jones, L., Kaiser, J. W., Kinne, S., Mangold, A., Razinger, M., Simmons, A. J., and Suttie, M.: Aerosol
649 analysis and forecast in the European Centre for Medium-Range Weather Forecasts Integrated Forecast
650 System: 2. Data assimilation, *J. Geophys. Res.*, 114, D13205, doi:10.1029/2008JD011115, 2009.
- 651 Brennan, J., Kaufman, Y., Koren, I., and Rong, L.: Aerosol-cloud interaction-Misclassification of MODIS
652 clouds in heavy aerosol, *IEEE T. Geosci. Remote*, 43, 911–915, doi:10.1109/TGRS.2005.844662, 2005.

653 Bennartz, R., and Rausch, J.: Global and regional estimates of warm cloud droplet number concentration
654 based on 13 years of AQUA-MODIS observations, *Atmos. Chem. Phys.*, 17, 9815-9836,
655 doi:10.5194/acp-17-9815-2017, 2017.

656 Bennartz, R.: Global assessment of marine boundary layer cloud droplet number concentration from satellite, *J.*
657 *Geophys. Res.*, 112, D02201, doi:10.1029/2006JD007547, 2007.

658 Boers, R., Acarreta, J. A., and Gras, J. L.: Satellite monitoring of the first indirect aerosol effect: Retrieval of
659 the droplet concentration of water clouds, *J. Geophys. Res.*, 111, D22208, doi:10.1029/2005JD006838,
660 2006.

661 Boucher, O., and Quaas, J.: Water vapour affects both rain and aerosol optical depth, *Nat. Geosci.*, 6, 4-5,
662 doi:10.1038/ngeo1692, 2012.

663 Chen, Q., Yin, Y., Jin, L., Xiao, H., and Zhu, S.: The effect of aerosol layers on convective cloud
664 microphysics and precipitation, *Atmos. Res.*, 101, 327-340, doi:10.1016/j.atmosres.2011.03.007, 2011.

665 Cheng, C. T., Wang, W. C., and Chen, J. P.: A modeling study of aerosol impacts on cloud microphysics and
666 radiative properties, *Q. J. R. Meteorol. Soc.*, 133, 283-297, doi:10.1002/qj.25, 2007.

667 Cheng, C. T., Wang, W. C., and Chen, J. P.: Simulation of the effects of increasing cloud condensation nuclei
668 on mixed-phase clouds and precipitation of a front system, *Atmos. Res.*, 96, 461-476, doi:
669 10.1016/j.atmosres.2010.02.005, 2010.

670 Chylek, P., Dubey, M. K., Lohmann, U., Ramanathan, V., Kaufman, Y. J., Lesins, G., Hudson, J., Altmann,
671 G., and Olsen, S.: Aerosol indirect effect over the Indian Ocean, *Geophys. Res. Lett.*, 33, L06806,
672 doi:10.1029/2005GL025397, 2006.

673 Dee, D. P., Uppala, S. M., Simmons, A. J., Berrisford, P., Poli, P., Kobayashi, S., Andrae, U., Balmaseda, M.
674 A., Balsamo, G., Bauer, P., Bechtold, P., Beljaars, A. C. M., van de Berg, L., Bidlot, J., Bormann, N.,
675 Delsol, C., Dragani, R., Fuentes, M., Geer, A. J., Haimberger, L., Healy, S. B., Hersbach, H., Hólm, E.
676 V., Isaksen, I., Kallberg, P., Köhler, M., Matricardi, M., McNally, A. P., Monge-Sanz, B. M.,
677 Morcrette, J.-J., Park, B.-K., Peubey, C., de Rosnay, P., Tavolato, C., Thépaut, J.-N., Vitart, F.: The
678 ERA-Interim reanalysis: configuration and performance of the data assimilation system, *Q. J. R.*
679 *Meteorol. Soc.*, 137, 553-597, doi:10.1002/qj.828, 2011.

680 Fan, J. W., Rosenfeld, D., Yang, Y., Zhao, C., Leung, L. R., and Li, Z. Q.: Substantial contribution of
681 anthropogenic air pollution to catastrophic floods in Southwest China, *Geophys. Res. Lett.*, 42,
682 6066-6075, doi:10.1002/2015GL064479, 2015.

683 Garrett, T. J. and Zhao, C.: Increased Arctic cloud longwave emissivity associated with pollution from
684 mid-latitudes, *Nature*, 440, 787-789, doi:10.1038/nature04636, 2006.

685 Givati, A., and Rosenfeld, D.: Quantifying precipitation suppression due to air pollution, *J. Appl. Meteor.*, 43,
686 1038-1056, doi:10.1175/1520-0450(2004)043<1038:QPSDTA>2.0.CO;2, 2004.

687 Grandey, B. S., and Stier, P.: A critical look at spatial scale choices in satellite-based aerosol indirect effect
688 studies, *Atmos. Chem. Phys.*, 10, 11459-11470, doi:10.5194/acp-10-11459-2010, 2010.

689 Grandey, B. S., Stier, P. and Wagner, T. M.: Investigating relationships between aerosol optical depth and
690 cloud fraction using satellite, aerosol reanalysis and general circulation model data, *Atmos. Chem. Phys.*,
691 13, 3177-3184, doi:10.5194/acp-13-3177-2013, 2013.

692 Gryspeerdt, E., Sourdeval, O., Quaas, J., Delanoë, J., Krämer, M., and Kühne, P.: Ice crystal number
693 concentration estimates from lidar–radar satellite remote sensing – Part 2: Controls on the ice crystal
694 number concentration, *Atmos. Chem. Phys.*, 18, 14351–14370, doi:10.5194/acp-18-14351-2018, 2018.

695 Gryspeerdt, E., Stier, P., and Grandey, B. S.: Cloud fraction mediates the aerosol optical depth–cloud top
696 height relationship, *Geophys. Res. Lett.*, 41, 3622-3627, doi:10.1002/2014GL059524, 2014a.

697 Gryspeerdt, E., Stier, P., and Partridge, D. G.: Links between satellite-retrieved aerosol and precipitation,
698 *Atmos. Chem. Phys.*, 14, 9677–9694, doi:10.5194/acp-14-9677-2014, 2014b.

699 Gunthe, S. S., Rose, D., Su, H., Garland, R. M., Achtert, P., Nowak, A., Wiedensohler, A., Kuwata, M.,
700 Takegawa, N., Kondo, Y., Hu, M., Shao, M., Zhu, T., Andreae, M. O., and Poschl, U.: Cloud
701 condensation nuclei (CCN) from fresh and aged air pollution in the megacity region of Beijing, *Atmos.*
702 *Chem. Phys.*, 11, 11023-11039, doi:10.5194/acp-11-11023-2011, 2011.

703 Guo, C. W., Xiao, H., Yang, H. L., and Tang, Q.: Observation and modeling analyses of the macro-and
704 microphysical characteristics of a heavy rain storm in Beijing, *Atmos. Res.*, 156, 125-141,
705 doi:10.1016/j.atmosres.2015.01.007, 2015.

706 Guo, J. P., Deng, M. J., Lee, S. S., Wang, F., Li, Z. Q., Zhai, P. M., Liu, H., Lv, W., Yao, W., and Li, X. W.:
707 Delaying precipitation and lightning by air pollution over the Pearl River Delta, Part I: Observational
708 analyses. *J. Geophys. Res.*, 121, 6472-6488, doi:10.1002/2015JD023257, 2016.

709 Guo, L., Highwood, E. J., Shaffrey, L. C., and Turner, A. G.: The effect of regional changes in anthropogenic
710 aerosols on rainfall of the East Asian Summer Monsoon, *Atmos. Chem. Phys.*, 13, 1521-1534,
711 doi:10.5194/acp-13-1521-2013, 2013.

712 Guo, X. L., Fu, D. H., Guo, X., and Zhang, C. M.: A case study of aerosol impacts on summer convective
713 clouds and precipitation over northern China, *Atmos. Res.*, 142, 142-157,
714 doi:10.1016/j.atmosres.2013.10.006, 2014.

715 Hammer, M. S., Martin, R. V., Li, C., Torres, O., Manning, M., and Boys, B. L.: Insight into global trends in
716 aerosol composition from 2005 to 2015 inferred from the OMI Ultraviolet Aerosol Index, *Atmos. Chem.*
717 *Phys.*, 18, 8097-8112, doi:10.5194/acp-18-8097-2018, 2018.

718 Harikishan, G., Padmakumari, B., Mahes Kumar, R. S., Pandithurai, G., and Min, Q. L.: Aerosol indirect effects
719 from ground-based retrievals over the rain shadow region in Indian subcontinent, *J. Geophys. Res.*, 121,
720 2369-2382, doi:10.1002/2015JD024577, 2016.

721 Higgins, R. W., Yao, Y., Yarosh, E. S., Janowiak, J. E. and Mo, K. C.: Influence of the Great Plains low-level
722 jet on summertime precipitation and moisture transport over the central United States, *J. Climate*, 10,
723 481-507, doi:10.1175/1520-0442(1997)010<0481:IOTGPL>2.0.CO;2, 1997.

724 Holz, R. E., Ackerman, S. A., Nagle, F. W., Frey, R., Dutcher, S., Kuehn, R. E., Vaughan, M. A., and Baum,

725 B.: Global Moderate Resolution Imaging Spectroradiometer (MODIS) cloud detection and height
726 evaluation using CALIOP, *J. Geophys. Res.*, 113, D00A19, doi: 10.1029/2008JD009837, 2008.

727 Jacobson, M. Z.: Strong radiative heating due to the mixing state of black carbon in atmospheric aerosols,
728 *Nature*, 409, 695-697, doi:10.1038/35055518, 2001.

729 Jiang, H., Feingold, G., and Cotton, W. R.: Simulations of aerosol-cloud-dynamical feedbacks resulting from
730 entrainment of aerosol into the marine boundary layer during the Atlantic Stratocumulus Transition
731 Experiment, *J. Geophys. Res.*, 107(D24), 4813, doi:10.1029/2001JD001502, 2002.

732 Jiang, J. H., Su, H., Schoeberl, M. R., Massie, S. T., Colarco, P., Platnick, S., and Livesey, N. J.: Clean and
733 polluted clouds: Relationships among pollution, ice clouds, and precipitation in South America, *Geophys.*
734 *Res. Lett.*, 35, L14804, doi: 10.1029/2008GL034631, 2008.

735 Jiang, M. J., Li, Z. Q., Wan, B. C., and Cribb, M.: Impact of aerosols on precipitation from deep convective
736 clouds in eastern China, *J. Geophys. Res.*, 121, 9607-9620, doi:10.1002/2015JD024246, 2016.

737 Johnson, D. B.: The role of giant and ultra-giant aerosol particles in warm rain initiation, *J. Atmos. Sci.*, 39,
738 448-460, doi:10.1175/1520-0469(1982)039<0448:TROGAU>2.0.CO;2, 1982.

739 Jung, W. S., Panicker, A. S., Lee, D. I., and Park, S. H.: Estimates of aerosol indirect effect from Terra
740 MODIS over Republic of Korea, *Advances in Meteorology*, 2013 (976813), 1-8,
741 doi:10.1155/2013/976813, 2013.

742 Kim, K. -M., Lau, K. M., Sud, Y. C., and Walker, G. K.: Influence of aerosol radiative forcings on the diurnal
743 and seasonal cycles of rainfall over West Africa and Eastern Atlantic Ocean using GCM simulation, *Clim.*
744 *Dyn.*, 35, 115-126, doi: 10.1007/s00382-010-0750-1, 2010.

745 Lau, K. M., Kim, M. K., and Kim, K. M.: Asian summer monsoon anomalies induced by aerosol direct
746 forcing: the role of the Tibetan Plateau, *Clim. Dyn.*, 26, 855-864, doi:10.1007/s00382-006-0114-z, 2006.

747 Lee, S. S., Donner, L. J., and Phillips, V. T. J.: Impacts of aerosol chemical composition on microphysics and
748 precipitation in deep convection, *Atmos. Res.*, 94, 220-237, doi:10.1016/j.atmosres.2009.05.015, 2009.

749 Lee, S. S., Guo, J., and Li, Z.: Delaying precipitation by air pollution over the Pearl River Delta: 2. Model
750 simulation, *J. Geophys. Res.*, 121, 11739-11760, doi:10.1002/2015JD024362, 2016.

751 Lelieveld, J. and Heintzenberg, J.: Sulfate cooling effect on climate through in-cloud oxidation of
752 anthropogenic SO₂, *Science*, 258, 117-120, doi:10.1126/science.258.5079.117, 1992.

753 Levy, R. C., Mattoo, S., Munchak, L. A., Remer, L. A., Sayer, A. M., Patadia, F., and Hsu, N. C.: The
754 Collection 6 MODIS aerosol products over land and ocean, *Atmos. Meas. Tech.*, 6, 2989-3034,
755 doi:10.5194/amt-6-2989-2013, 2013.

756 Li, H., Cui, X., Zhang, W., and Qiao, L.: Observational and dynamic downscaling analysis of a heavy rainfall
757 event in Beijing, China during the 2008 Olympic Games, *Atmos. Sci. Lett.*, 17, 368-376,
758 doi:10.1002/asl.667, 2016.

759 Li, Z., Niu, F., Fan, J., Liu, Y., Rosenfeld, D., and Ding, Y.: Long-term impacts of aerosols on the vertical
760 development of clouds and precipitation, *Nat. Geosci.*, 4, 888-894, doi:10.1038/ngeo1313, 2011.

761 Lim, K. S. and Hong, S.: Investigation of aerosol indirect effects on simulated flash-flood heavy rainfall over
762 Korea, *Meteor. Atmos. Phys.*, 118, 199-214, doi:10.1007/s00703-012-0216-6, 2012.

763 Liu, G., Shao, H., Coakley Jr. J. A., Curry, J. A., Haggerty, J. A., and Tschudi, M. A.: Retrieval of cloud
764 droplet size from visible and microwave radiometric measurements during INDOEX: Implication to
765 aerosols' indirect radioactive effect, *J. Geophys. Res.*, 108(D1), 4006, doi:10.1029/2001JD001395, 2003.

766 Liu, J., Wang, S., Zhang, W., and Wei, X.: Mechanism analysis of a strong convective weather in Hebei
767 Province, *Advances in Marine Science*, 30, 9-16, 2012. (in Chinese)

768 Menzel, W. P., Frey, R. A., Zhang, H., Wylie, D. P., Moeller, C. C., Holz, R. E., Maddux, B., Baum, B. A.,
769 Strabala, K. I., and Gumley, L. E.: MODIS global cloud-top pressure and amount estimation: Algorithm
770 description and results, *J. Appl. Meteorol. Clim.*, 47, 1175-1198, doi: 10.1175/2007JAMC1705.1, 2008.

771 Min, Q., Joseph, E., Lin, Y., Min, L., Yin, B., Daum, P. H., Kleinman, L. I., Wang, J., and Lee, Y. -N.:
772 Comparison of MODIS cloud microphysical properties with in-situ measurements over the Southeast
773 Pacific, *Atmos. Chem. Phys.*, 12, 11261-11273, doi:10.5194/acp-12-11261-2012, 2012.

774 Nakajima, T. and King, M. D.: Determination of the optical thickness and effective particle radius of clouds
775 from reflected solar radiation measurements. Part I: Theory, *J. Atmos. Sci.*, 47, 1878-1893,
776 doi:10.1175/1520-0469(1990)047<1878:DOTOTA>2.0.CO;2, 1990.

777 Panicker, A. S., Pandithurai, G., and Dipu, S.: Aerosol indirect effect during successive contrasting monsoon
778 seasons over Indian subcontinent using MODIS data, *Atmos. Environ.*, 44, 1937-1943,
779 doi:10.1016/j.atmosenv.2010.02.015, 2010.

780 Platnick, S., Meyer, K., King, M. D., Wind, G., Amarasinghe, N., Marchant, B., Arnold, G. T., Zhang, Z.,
781 Hubanks, P. A., Holz, R. E., Yang, P., Ridgway, W. L., and Riedi, J.: The MODIS cloud optical and
782 microphysical products: Collection 6 updates and examples from Terra and Aqua, *IEEE Trans. Geosci.*
783 *Remote Sens.*, 55, 502-525, doi:10.1109/TGRS.2016.2610522, 2017.

784 Qian, Y., Gong, D. Y., Fan, J. W., Leung, L. R., Bennartz, R., Chen, D. L., Wang, W. G.: Heavy pollution
785 suppresses light rain in China: Observations and modeling, *J. Geophys. Res.*, 114, D00K02,
786 doi:10.1029/2008JD011575, 2009.

787 Qiu, Y., Zhao, C., Guo, J., and Li, J.: 8-Year ground-based observational analysis about the seasonal variation
788 of the aerosol-cloud droplet effective radius relationship at SGP site, *Atmos. Environ.*, 164, 139-146,
789 doi:10.1016/j.atmosenv.2017.06.002, 2017.

790 Quaas, J., Boucher, O., Bellouin, N. and Kinne, S.: Satellite-based estimate of the direct and indirect aerosol
791 climate forcing, *J. Geophys. Res.*, 113, D05204, doi:10.1029/2007JD008962, 2008.

792 Quaas, J., Stevens, B., Stier, P., and Lohmann U.: Interpreting the cloud cover aerosol optical depth
793 relationship found in satellite data using a general circulation model, *Atmos. Chem. Phys.*, 10, 6129-6135,
794 doi:10.5194/acp-10-6129-2010, 2010.

795 Reutter, P., Su, H., Trentmann, J., Simmel, M., Rose, D., Gunthe, S. S., Wernli, H., Andreae, M. O., and
796 Po ¨schl, U.: Aerosol- and updraft-limited regimes of cloud droplet formation: influence of particle

797 number, size and hygroscopicity on the activation of cloud condensation nuclei (CCN), *Atmos. Chem.*
798 *Phys.*, 9, 7067-7080, doi:10.5194/acp-9-7067-2009, 2009.

799 Rienecker, M. M., Suarez, M. J., Todling, R., Bacmeister, J., Takacs, L., Liu, H. C., Gu, W., Sienkiewicz, M.,
800 Koster, R. D., Gelaro, R., Stajner, I., Nielsen, J. E.: The GEOS-5 Data Assimilation
801 System—Documentation of Versions 5.0.1 and 5.1.0, and 5.2.0. NASA Technical Report Series on
802 Global Modeling and Data Assimilation NASA/TM-2008 -104606 27: 92 pp, 2008.

803 Rosenfeld, D.: TRMM observed first direct evidence of smoke from forest fires inhibiting rainfall, *Geophys.*
804 *Res. Lett.*, 26, 3105–3108, doi:10.1029/1999GL006066, 1999.

805 Rosenfeld, D., Lohmann, U., Raga, G. B., O'Dowd, C. D., Kulmala, M., Fuzzi, S., Reissell, A., Andreae, M.
806 O.: Flood or drought: How do aerosols affect precipitation? *Science*, 321, 1309-1313,
807 doi:10.1126/science.1160606, 2008.

808 Rosenfeld, D., Sherwood, S., Wood, R., and Donner, L.: Climate effects of aerosol-cloud interactions, *Science*,
809 343, 379-380, doi:10.1126/science.1247490, 2014.

810 Rosenfeld, D., and Woodley, W. L.: Convective clouds with sustained highly supercooled liquid water down
811 to -37.5°C, *Nature*, 405, 440–442, doi:10.1038/35013030, 2000.

812 Sassen, K., Starr, D., Mace, G. G., Poellot, M. R., Melfi, S. H., Eberhard, W.L., Spinhirne, J. D., Eloranta, E.
813 W., Hagan, D. E., and Hallett, J.: The 5–6 December 1991 FIRE IFO II jet stream cirrus case study:
814 Possible influences of volcanic aerosols, *J. Atmos. Sci.*, 52, 97–123, doi:10.1175/1520-0469(1995)
815 052<0097:TDFIJJ>2.0.CO;2, 1995.

816 Shen, Y., Xiong, A., Wang, Y., and Xie, P.: Performance of high-resolution satellite precipitation products
817 over China, *J. Geophys. Res.*, 115, D02114, doi:10.1029/2009JD012097, 2010.

818 Sherwood, S.: Aerosols and ice particle size in tropical cumulonimbus, *J. Clim.*, 15, 1051–1063,
819 doi:10.1175/1520-0442(2002)015<1051:AAIPSI>2.0.CO;2, 2002.

820 Shinozuka, Y., Clarke, A. D., Nenes, A., Jefferson, A., Wood, R., McNaughton, C. S., Ström, J., Tunved, P.,
821 Redemann, J., Thornhill, K. L., Moore, R. H., Latham, T. L., Lin, J. J., and Yoon, Y. J.: The relationship
822 between cloud condensation nuclei (CCN) concentration and light extinction of dried particles:
823 indications of underlying aerosol processes and implications for satellite-based CCN estimates, *Atmos.*
824 *Chem. Phys.*, 15, 7585-7604, doi:10.5194/acp-15-7585-2015, 2015.

825 Song, X. L. and Zhang, G. J.: Microphysics parameterization for connective clouds in a global climate model:
826 Description and single-column model tests, *J. Geophys. Res.*, 116, D02201, doi:10.1029/2010JD014833,
827 2011.

828 Squires, P.: The growth of cloud drops by condensation: I. general characteristics, *Aust. J. Sci. Res., Ser. A*, 5,
829 66–86, 1952.

830 Squires, P., and Twomey, S.: A comparison of cloud nucleus measurements over central North America and
831 Caribbean Sea, *J. Atmos. Sci.*, 23, 401–404, doi: 10.1175/1520-0469(1966)023<0401:ACOCNM>
832 -2.0.CO;2, 1966.

833 Sun, Y. L., Wang, Z. F., Du, W., Zhang, Q., Wang, Q. Q., Fu, P. Q., Pan, X. L., Li, J., Jayne, J., and Worsnop,
834 D. R.: Long-term real-time measurements of aerosol particle composition in Beijing, China: seasonal
835 variations, meteorological effects, and source analysis, *Atmos. Chem. Phys.*, 15, 10149-10165,
836 doi:10.5194/acp-15-10149-2015, 2015.

837 Tariq, S., and Ali, M.: Spatio-temporal distribution of absorbing aerosols over Pakistan retrieved from OMI on
838 board Aura Satellite, *Atmos. Pollution Res.*, doi: 10.5094/APR.2015.030, 2015.

839 Tao, M. H., Chen, L. F., Wang, Z. F., Tao, J. H., Che, H. Z., Wang, X. H., and Wang, Y.: Comparison and
840 evaluation of the MODIS Collection 6 aerosol data in China, *J. Geophys. Res.*, 120, 6992-7005,
841 doi:10.1002/2015JD023360, 2015.

842 Tao, W. K., Chen, J. P., Li, Z., Wang, C., and Zhang C.: Impact of aerosols on convective clouds and
843 precipitation, *Rev. Geophys.*, 50, RG2001/2012, 1-62, doi: 10.1029/2011RG000369, 2012.

844 Torres, O., Bhartia, P.K., Herman, J.R., Ahmad, Z., Gleason, J.: Derivation of aerosol properties from satellite
845 measurements of backscattered ultraviolet radiation: Theoretical basis, *J. Geophys. Res.*, 103, 17099–
846 17110, doi:10.1029/98JD00900, 1998.

847 Twohy, C. H., Coakley, J. A., and Tahnk, W. R.: Effect of changes in relative humidity on aerosol scattering
848 near clouds, *J. Geophys. Res.*, 114, D05205, doi:10.1029/2008JD010991, 2009.

849 Twomey, S.: The influence of pollution on the shortwave albedo of clouds, *J. Atmos. Sci.*, 34, 1149–1152,
850 doi:10.1175/1520-0469(1977)034<1149:TIOPOT>2.0.CO;2, 1977.

851 Wang, J., Feng, J., Wu, Q., and Z. Yan, Z.: Impact of anthropogenic aerosols on summer precipitation in the
852 Beijing-Tianjin-Hebei urban agglomeration in China: Regional climate modeling using WRF-Chem, *Adv.*
853 *Atmos. Sci.*, 33, 753-766, doi:10.1007/s00376-015-5103-x, 2016.

854 Wolyn, P. G., and Mckee, T. B.: The mountain plains circulation east of a 2-km-high north south barrier, *Mon.*
855 *Weather Rev.*, 122, 1490-1508, doi:10.1175/1520-0493(1994)122<1490:TMPCEO>2.0.CO;2, 1994.

856 Wu, P., Ding, Y. H., and Liu, Y. J.: Atmospheric circulation and dynamic mechanism for persistent haze
857 events in the Beijing-Tianjin-Hebei region, *Adv. Atmos. Sci.*, 34, 429-440,
858 doi:10.1007/s00376-016-6158-z, 2017.

859 Yang, X., Zhao, C., Zhou, L., Li, Z., Cribb, M., and Yang, S.: Wintertime cooling and a potential connection
860 with transported aerosols in Hong Kong during recent decades, *Atmos. Res.*, 211, 52-61,
861 doi:10.1016/j.atmosres.2018.04.029, 2018.

862 Yu, R. C., Zhou, T. J., Xiong, A. Y., Zhu, Y. J., and Li, J. M.: Diurnal variations of summer precipitation over
863 contiguous China, *Geophys. Res. Lett.*, 34, L017041, doi:10.1029/2006GL028129, 2007.

864 Yuan, T., Li, Z., Zhang, R., and Fan, J.: Increase of cloud droplet size with aerosol optical depth: An
865 observation and modeling study, *J. Geophys. Res.*, 113, D04201, doi:10.1029/2007JD008632, 2008.

866 Yuan, W. H., Yu, R. C., Chen, H. M., Li, J., and Zhang, M. H.: Subseasonal Characteristics of Diurnal
867 Variation in Summer Monsoon Rainfall over Central Eastern China, *J. Climate*, 23, 6684-6695,
868 doi:10.1175/2010JCLI3805.1, 2010.

869 Zeng, S., Riedi, J., Trepte, C. R., Winker, D. M., and Hu, Y. -X.: Study of global cloud droplet number
870 concentration with A-Train satellites, *Atmos. Chem. Phys.*, 14, 7125-7134, doi:
871 10.5194/acp-14-7125-2014, 2014.

872 Zhao, B., Gu, Y., Liou, K. -N., Wang, Y., Liu, X., Huang, L., Jiang, J. H., and Su, H.: Type-Dependent
873 Responses of Ice Cloud Properties to Aerosols From Satellite Retrievals, *Geophys. Res. Lett.*, 45, 3297–
874 3306, doi:10.1002/2018GL077261, 2018.

875 Zhou, S., Yang, J., Wang, W. C., Gong, D., Shi, P., and Gao, M.: Shift of daily rainfall peaks over the
876 Beijing–Tianjin–Hebei region: An indication of pollutant effects? *Int. J. Climatol.* 2018;1–10,
877 doi:10.1002/joc.5700, 2018.

878 Zhu, Y., Rosenfeld, D., and Li, Z.: Under what conditions can we trust retrieved cloud drop concentrations in
879 broken marine stratocumulus? *J. Geophys. Res.*, 123, 8754-8767, doi:10.1029/2017JD028083, 2018.

880

881 **Tables**

882

Indicator	Source	Begin time	Thresholds	
			25 th percentile	75 th percentile
AOD	MODIS	2002	0.98	2.00
CDNC (cm ⁻³)	MODIS	2002	80.70	199.08
AAI	OMI	2005	0.13	0.52
SAI	OMI	2005	- 0.13	- 0.35
AOD of BC	MACC	2003	0.04	0.06
AOD of sulfate	MACC	2003	0.46	0.87
SH at 850 hPa (g/kg)	ERA-interim	2002	9.96	12.95

883

884 Table 1. The indicators of aerosols and moisture used in the study and their sources, begin times and the
885 thresholds (25th and 75th percentiles). The end time of all data is to 2012.

886

887

888

889

Characteristics of heavy rainfall	Clean		Polluted		Difference		Significance	
	AOD	CDNC	AOD	CDNC	AOD	CDNC	AOD	CDNC
Start time	24.2 (3.9)	22.4 (4.3)	23.5 (4.8)	20.2 (4.1)	- 0.7	- 2.2	P<0.05	P<0.05
Peak time	23.0 (4.0)	22.2 (5.7)	22.0 (4.8)	19.6 (5.4)	- 1.0	- 2.6	P<0.05	P<0.05
Duration	4.0 (2.1)	5.9 (3.7)	4.8 (2.8)	6.4 (3.9)	0.8	0.5	P<0.05	P<0.05
Intensity	164.9 (98.4)	166.4 (92.4)	169.6 (94.3)	163.2 (90.0)	4.7	- 3.2	P>0.1	P>0.1

890

891 Table 2. The mean values of start time (units: LST), peak time (units: LST), duration (units: hours) and
892 intensity (units: 0.1mm/hour) of heavy rainfall respectively on the clean and polluted conditions using two
893 indicators of AOD and CDNC, and their differences (polluted minus clean) and significances. The numbers in
894 the brackets stand for the standard deviations on the means. “P<0.05” stands for the difference has passed the
895 significance test of 95%, and “P>0.1” stands for the difference did not pass the significance test of 90%.

896

897

Characteristics of heavy rainfall	AAI	SAI	Difference (AAI-SAI)	Less BC	More BC	Difference (More-Less)	Less sulfate	More sulfate	Difference (More-Less)
Start time	23.4 (4.8)	24.1 (4.4)	-0.7	24.2 (4.8)	23.9 (4.4)	-0.3	24.0 (4.3)	24.5 (4.4)	0.5
Peak time	21.0 (5.3)	22.6 (5.1)	-1.6	23.4 (5.3)	22.3 (4.0)	-1.1	23.2 (4.5)	22.9 (4.8)	-0.3
Duration	5.0 (3.1)	6.0 (3.8)	-1.0	4.8 (2.6)	4.6 (2.7)	-0.2	4.0 (2.1)	5.5 (3.0)	1.5

898

899 Table 3. The mean values of start time (units: LST), peak time (units: LST) and duration (units: hours) of
900 heavy rainfall respectively on the conditions with more absorbing aerosols (AAI more than 75th percentile,
901 from OMI), more scattering aerosols (SAI more than 75th percentile, from OMI), less or more BC (AOD of
902 BC less than 25th or more than 75th percentile, from MACC), less or more sulfate (AOD of sulfate less than
903 25th or more than 75th percentile, from MACC), and their differences. Numbers in the brackets stand for the
904 standard deviations on the means. All differences have passed the significant test of 95%.

905

906

907

908

Clean/Polluted	CF	CTP	COT		CWP		CER		
			liquid	ice	liquid	ice	liquid	ice	
AOD	Clean	62.8 (17.6)	442.3 (149.6)	6.9 (4.5)	6.7 (8.5)	62.8 (36.6)	123.1 (168.9)	16.7 (4.4)	32.0 (8.7)
	Polluted	89.3 (12.9)	487.3 (145.7)	10.0 (5.8)	12.9 (17.0)	96.4 (52.5)	211.3 (279.3)	17.5 (3.5)	29.2 (9.0)
CDNC	Clean	95.4 (5.7)	369.9 (110.0)	11.7 (12.9)	8.7 (13.6)	153.2 (159.0)	238.0 (281.9)	20.0 (2.8)	34.1 (5.5)
	Polluted	96.9 (4.7)	460.1 (145.6)	28.4 (22.3)	33.1 (22.6)	265.6 (210.4)	462.1 (443.5)	12.5 (2.0)	24.6 (8.9)

909

910

911

912

913

914

915

916

917

918

919

Table 4. The mean values of CF (units: %), CTP (units: hPa), COT (liquid and ice, units: none), CWP (liquid and ice, units: g/m²) and CER (liquid and ice, units: μm) from MODIS C6 cloud product on the clean condition (less than 25th percentile) and polluted condition (more than 75th percentile) using two indicators of AOD and CDNC. Numbers in the brackets stand for the standard deviations on the means. Numbers in grey indicate the results of liquid COT & CER are related to the calculation of CDNC. The differences between clean and polluted conditions have all passed the significant test of 95%.

Group (case number)	CF	CTP	COT		CWP		CER	
			liquid	ice	liquid	ice	liquid	ice
1.Clean, dry (123)	91.7 (6.8)	413.5 (129.4)	9.9 (9.0)	7.9 (8.9)	119.9 (122.7)	163.2 (180.9)	19.9 (2.8)	35.7 (6.2)
2.Polluted, dry (140)	96.0 (4.9)	493.6 (140.1)	39.2 (24.6)	37.3 (22.4)	311.0 (233.3)	683.5 (458.0)	12.5 (2.1)	28.3 (8.2)
3.Clean, wet (178)	95.6 (6.0)	464.3 (131.1)	19.2 (17.9)	18.0 (17.9)	219.4 (216.5)	354.9 (364.3)	<i>19.2 (2.7)</i> <i>p_{1,3}>0.05</i>	32.7 (4.3)
4.Polluted, wet (195)	97.5 (4.7)	<i>462.7 (156.4)</i> <i>p_{3,4}>0.05</i>	32.2 (22.0)	24.6 (21.4)	259.0 (219.1)	393.3 (418.3)	12.8 (2.1)	24.0 (8.2)

920

921

922

923

924

925

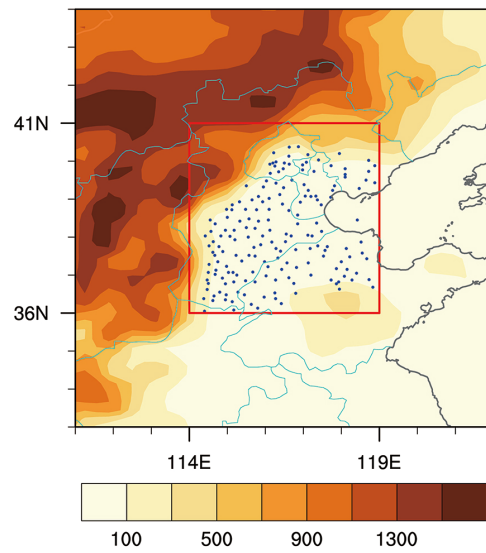
926

927

Table 5. The mean values of CF (units: %), CTP (units: hPa), COT (liquid and ice, units: none), CWP (liquid and ice, units: g/m²) and CER (liquid and ice, units: μm) in four groups. Numbers in the brackets stand for the standard deviations on the means. Italic numbers in grey represent that the differences are not significant, in which “P>0.05” stands for the difference did not pass the significance test of 95%.

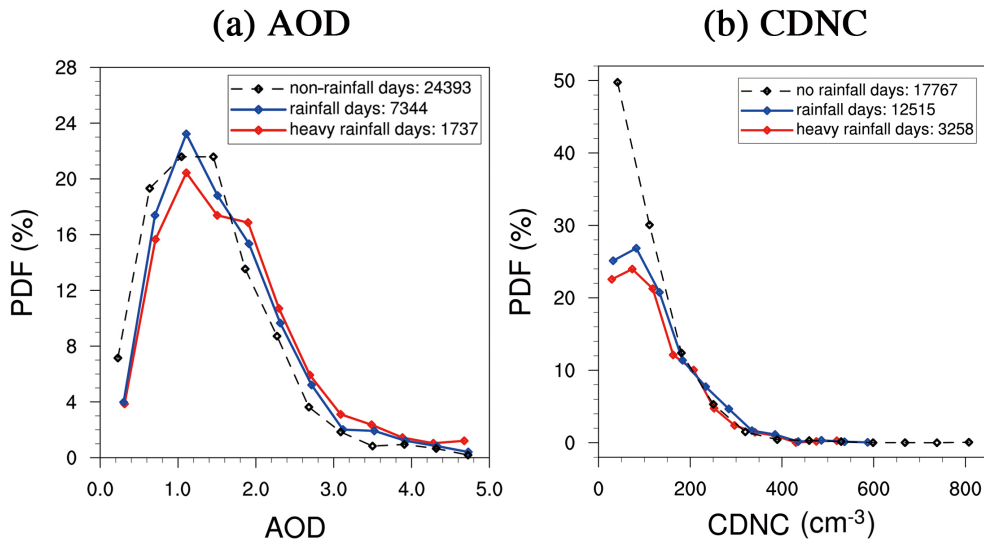
928
929
930
931
932
933
934
935
936
937
938
939
940
941
942
943
944
945
946
947
948

Figures



949
950
951
952

Figure 1. Selected rainfall stations (blue dots) and topography (shading, units: m) in the BTH region (red box, 36–41° N, 114–119° E).



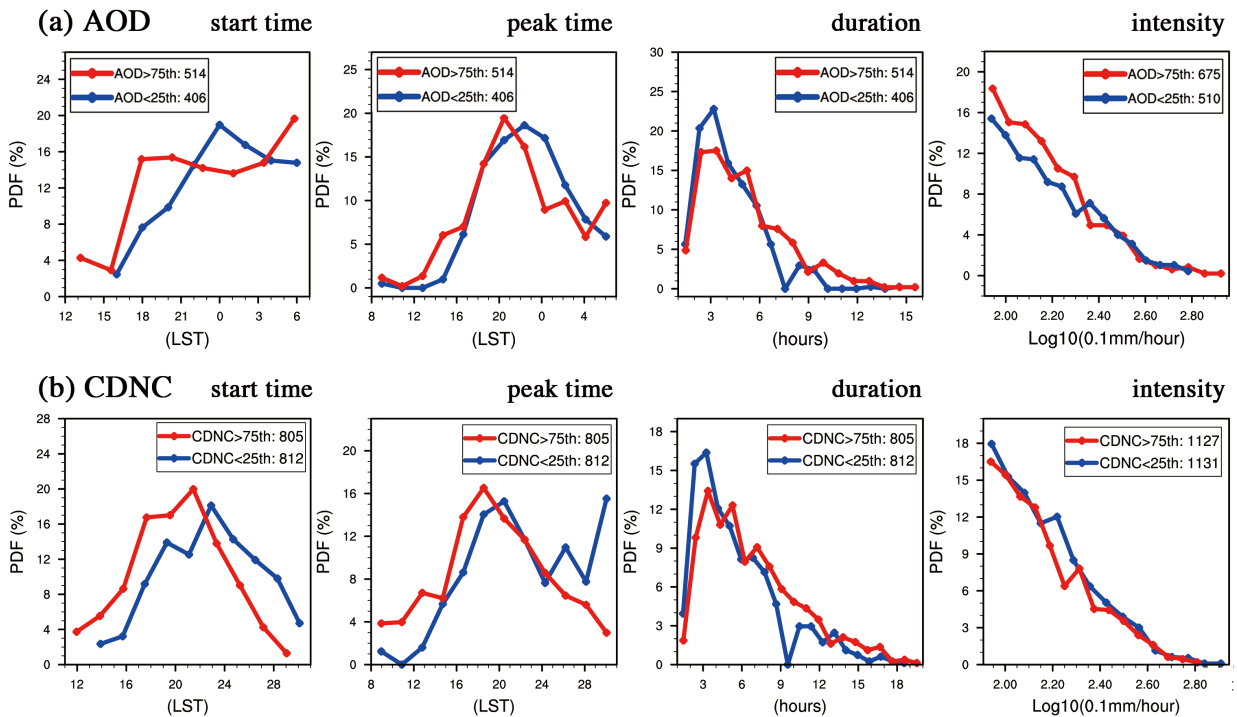
954

955 Figure 2. PDF of (a) AOD and (b) CDNC (cm⁻³) (data from MODIS) on non-rainfall days (black lines),
 956 rainfall days (blue lines) and heavy rainfall days (red lines) in southwesterly during early summers from 2002
 957 to 2012. Numbers in the legends denote the sample number.

958

959

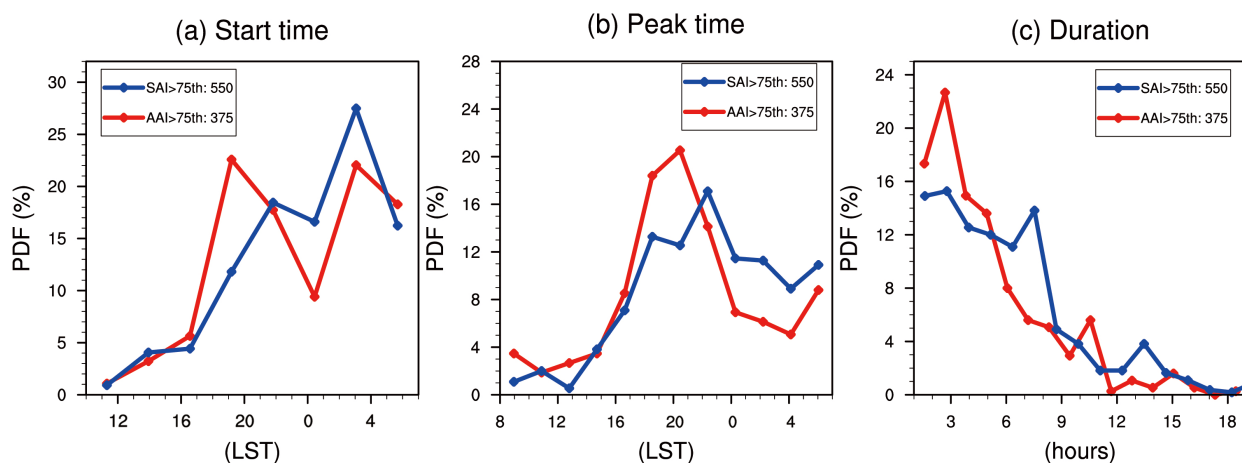
960



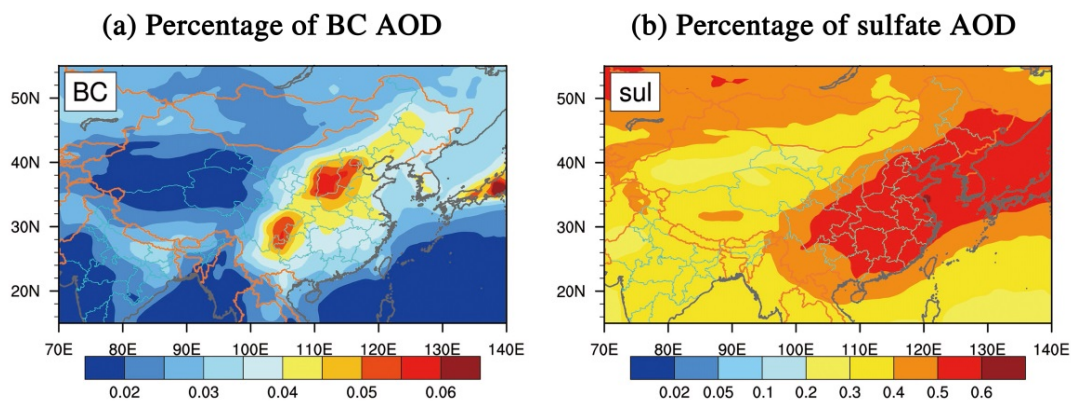
961

962 Figure 3. PDF of start time (units: LST), peak time (units: LST), duration (units: hours) and intensity (units:

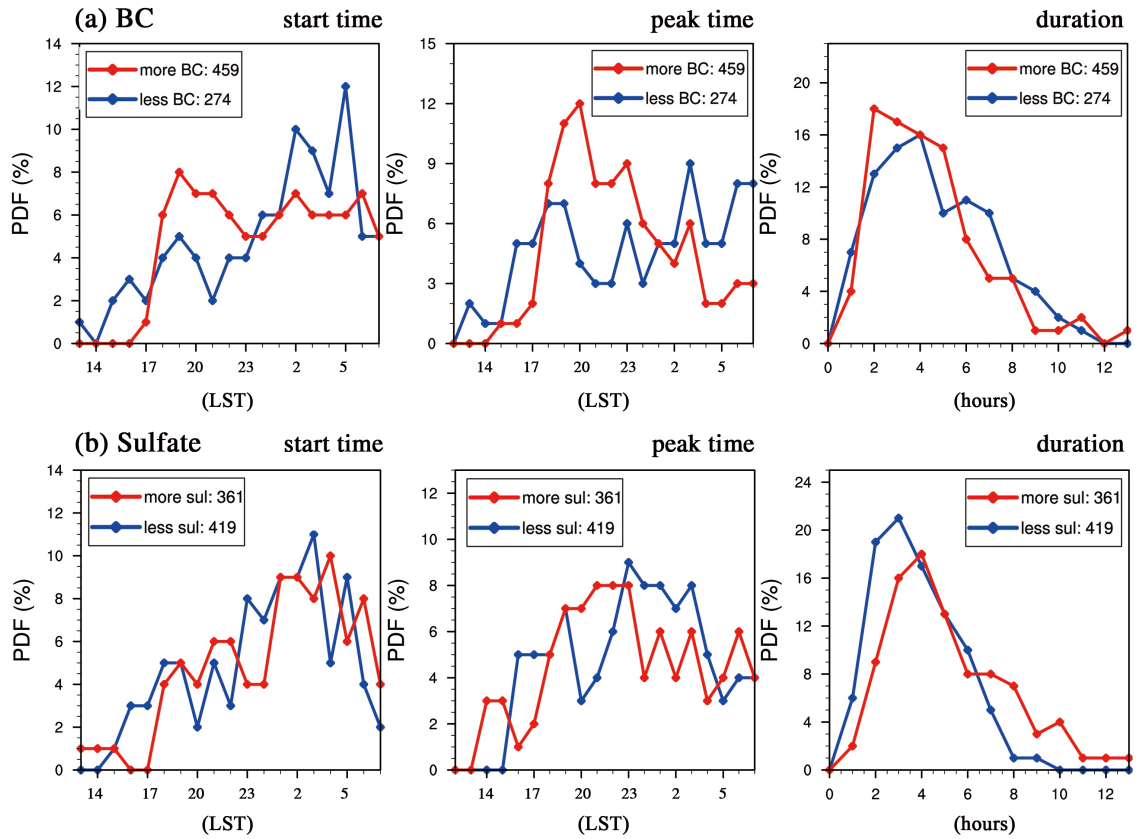
963 0.1mm/hour) of heavy rainfall (data from CMA) on selected clean (blue lines) and polluted (red lines)
 964 conditions, respectively using indicator of (a) AOD and (b) CDNC (cm^{-3}), during early summers from 2002 to
 965 2012.
 966



967
 968 Figure 4. PDF of (a) start time (units: LST), (b) peak time (units: LST), and (c) duration (units: hours) of
 969 heavy rainfall on the days with SAI more than 75th percentile (blue lines, data from OMI) and days with AAI
 970 more than 75th percentile (red lines, data from OMI), during early summers from 2005 to 2012.
 971
 972



973
 974 Figure 5. Percentages of AOD for (a) BC and (b) sulfate from MACC reanalysis data in summers (June –
 975 August) during 2002 to 2012.
 976
 977
 978



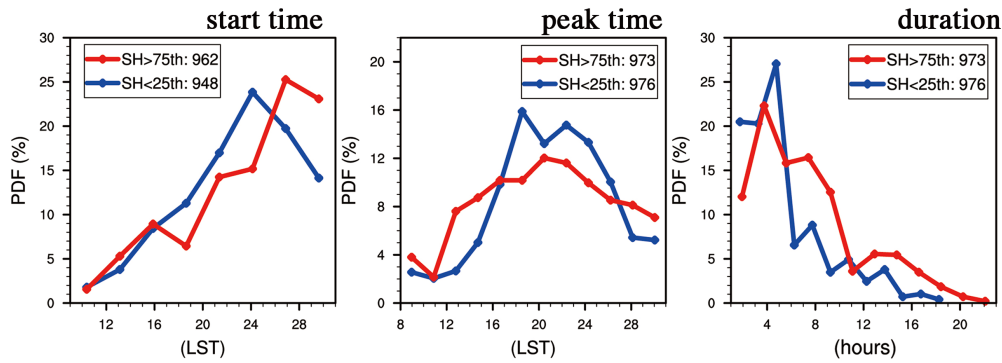
979

980 Figure 6. PDF of start time (units: LST), peak time (units: LST) and duration (units: hours) of heavy rainfall
 981 on the different conditions of (a) BC and (b) sulfate. Blue/red lines stand for the condition of less/more BC or
 982 sulfate (AOD of BC or sulfate less than 25th /more than 75th percentile, data from MACC) during early
 983 summers from 2003 to 2012.

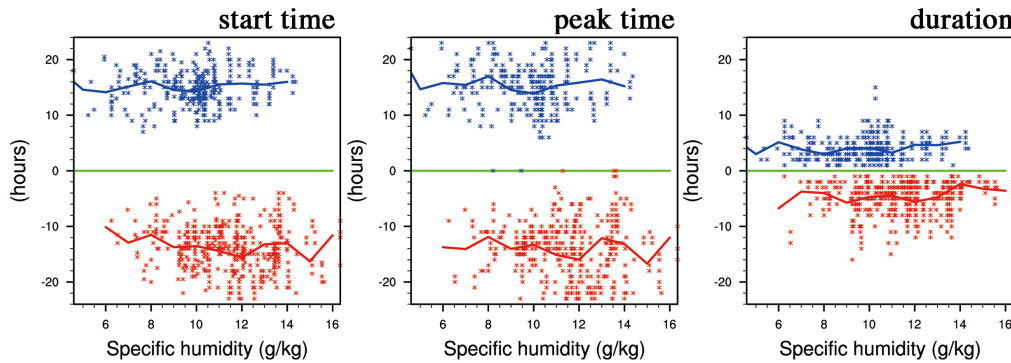
984

985

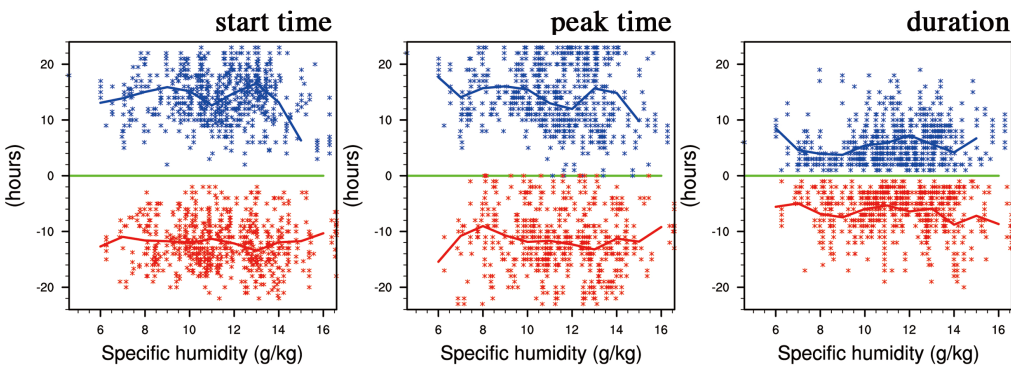
(a) PDF with more/less SH



(b) Scatter distribution using AOD



(c) Scatter distribution using CDNC

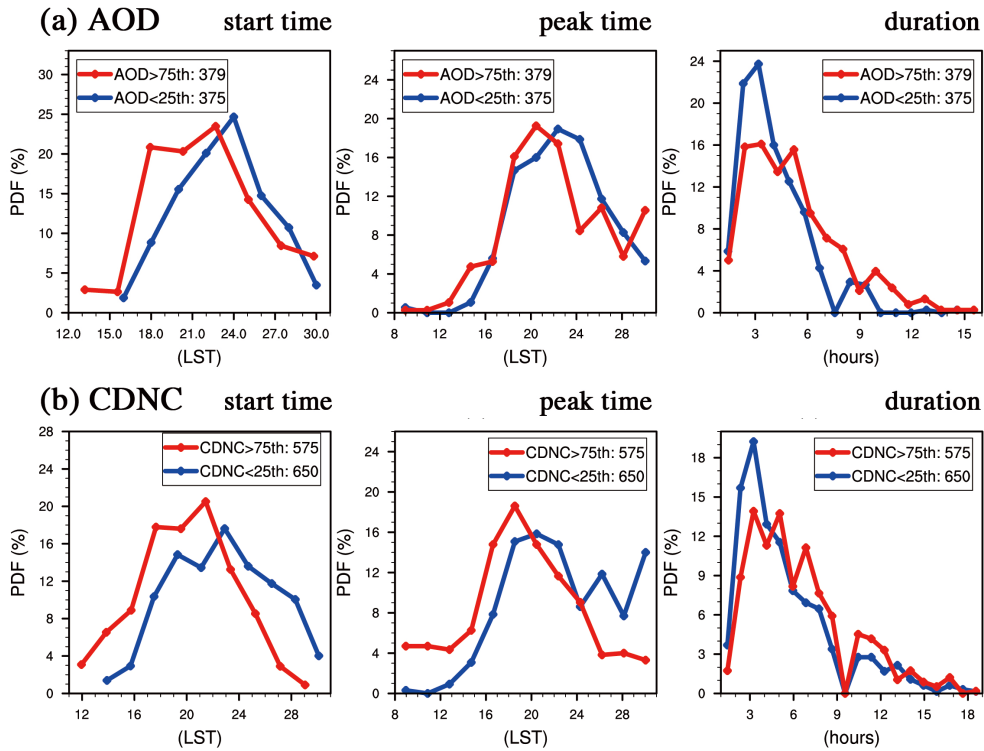


986

987 Figure 7. (a) PDF of start time (units: LST), peak time (units: LST), and duration (units: hours) of heavy
 988 rainfall with less moisture (blue lines, SH at 850 hPa less than 25th percentile, data form ERA-interim) and
 989 more moisture (red lines, SH at 850 hPa more than 75th percentile, data form ERA-interim). (b) and (c) are
 990 scatter distributions of SH-start time/peak time/duration for clean cases (blue points) and polluted cases (red
 991 points) respectively using AOD and CDNC. Green lines stands for the start/peak time at 8:00 LST or the
 992 duration is 0 hours. Positive (negative) values stand for the hours away from 8:00 LST or 0 hours in clean
 993 (polluted) cases. Blue (red) lines stand for the mean values of rainfall characteristics at each integer of SH in
 994 clean (polluted) cases.

995

996



997

998

999 Figure 8. PDF of start time (units: LST), peak time (units: LST), and duration (units: hours) of heavy rainfall
.000 on selected clean (blue lines) and polluted (red lines) conditions with SH at 850 hPa (from ERA-interim) less
.001 than 75th percentile, respectively using indicator of (a) AOD and (b) CDNC (cm⁻³), during early summers from
.002 2002 to 2012.

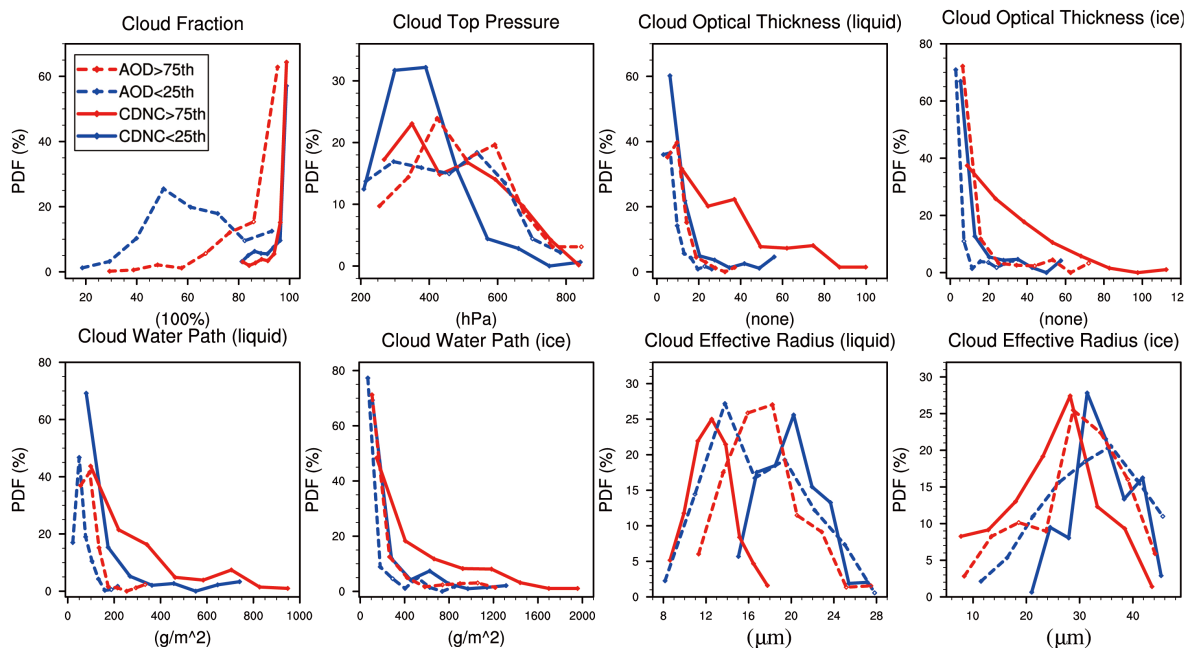
.003

.004

.005

.006

.007



.008

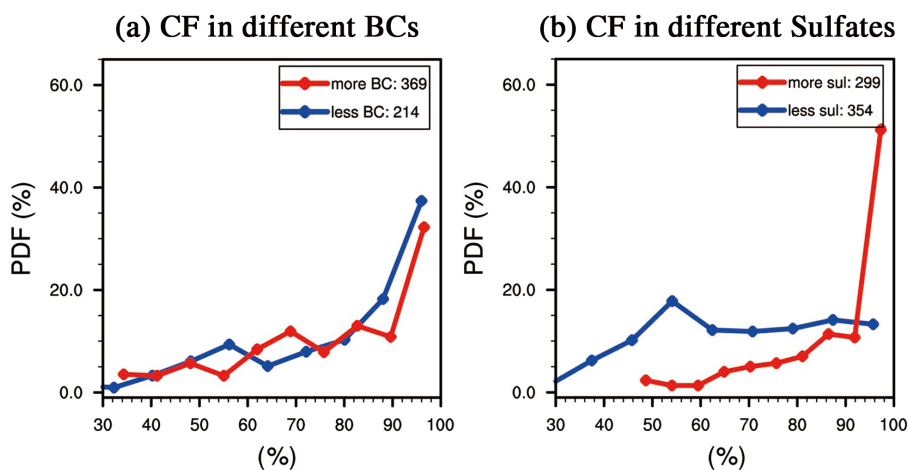
.009 Figure 9. PDF of CF (units: %), CTP (units: hPa), COT (liquid and ice, units: none), CWP (liquid and ice,
 .010 units: g/m^2) and CER (liquid and ice, units: μm) on selected clean (blue dash lines: AOD<25th percentile; blue
 .011 solid lines: CDNC<25th percentile) and polluted (red dash lines: AOD>75th percentile; red solid lines:
 .012 CDNC>75th percentile) heavy rainfall days. All cloud variables are obtained from MODIS C6 cloud product.

.013

.014

.015

.016



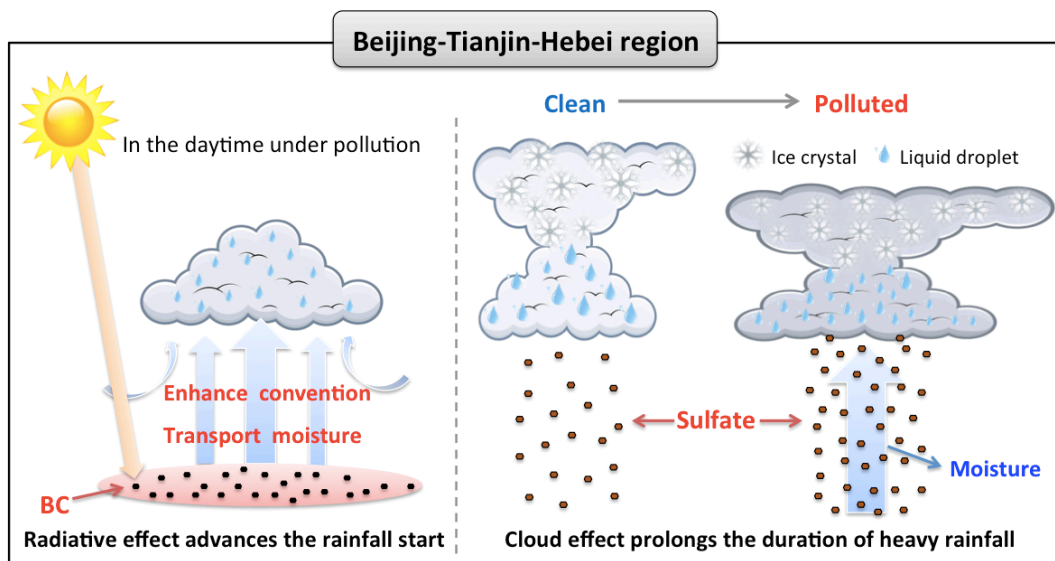
.017

.018 Figure 10. PDF of CF (units: %, data from MODIS) respectively for the conditions of less BC/sulfate (blue
 .019 lines, AOD of BC/sulfate less than 25th percentile, data from MACC) and more BC/sulfate (red lines, AOD of
 .020 BC/sulfate more than 75th percentile, data from MACC) cases with heavy rainfall during 10 early summers
 .021 (2003-2012).

.022

.023

.024



.025

.026

.027

.028

.029

Figure 11. A schematic diagram for aerosol impacts on heavy rainfall over Beijing-Tianjin-Hebei region.